RESEARCH ARTICLE

The KRAS^{G12C} Inhibitor MRTX849 Provides Insight toward Therapeutic Susceptibility of KRAS-Mutant Cancers in Mouse Models and Patients

Jill Hallin[1], Lars D. Engstrom[1], Lauren Hargis[1], Andrew Calinisan[1], Ruth Aranda[1], David M. Briere[1], Niranjan Sudhakar[1], Vickie Bowcut[1], Brian R. Baer[2], Joshua A. Ballard[2], Michael R. Burkard[2], Jay B. Fell[2], John P. Fischer[2], Guy P. Vigers[2], Yaohua Xue[3], Sole Gatto[4], Julio Fernandez-Banet[4], Adam Pavlicek[4], Karen Velastagui[1], Richard C. Chao[1], Jeremy Barton[1], Mariaelena Pierobon[5], Elisa Baldelli[5], Emanuel F. Patricoin III[5], Douglas P. Cassidy[6], Matthew A. Marx[1], Igor I. Rybkin[7], Melissa L. Johnson[8], Sai-Hong Ignatius Ou[9], Piro Lito[3], Kyriakos P. Papadopoulos[10], Pasi A. Jänne[6], Peter Olson[1], and James G. Christensen[1]

ABSTRACT Despite decades of research, efforts to directly target KRAS have been challenging. MRTX849 was identified as a potent, selective, and covalent KRAS^{G12C} inhibitor that exhibits favorable drug-like properties, selectively modifies mutant cysteine 12 in GDP-bound KRAS^{G12C}, and inhibits KRAS-dependent signaling. MRTX849 demonstrated pronounced tumor regression in 17 of 26 (65%) KRAS^{G12C}-positive cell line– and patient-derived xenograft models from multiple tumor types, and objective responses have been observed in patients with KRAS^{G12C}-positive lung and colon adenocarcinomas. Comprehensive pharmacodynamic and pharmacogenomic profiling in sensitive and partially resistant nonclinical models identified mechanisms implicated in limiting antitumor activity including KRAS nucleotide cycling and pathways that induce feedback reactivation and/or bypass KRAS dependence. These factors included activation of receptor tyrosine kinases (RTK), bypass of KRAS dependence, and genetic dysregulation of cell cycle. Combinations of MRTX849 with agents that target RTKs, mTOR, or cell cycle demonstrated enhanced response and marked tumor regression in several tumor models, including MRTX849-refractory models.

SIGNIFICANCE: The discovery of MRTX849 provides a long-awaited opportunity to selectively target KRAS^{G12C} in patients. The in-depth characterization of MRTX849 activity, elucidation of response and resistance mechanisms, and identification of effective combinations provide new insight toward KRAS dependence and the rational development of this class of agents.

See related commentary by Klempner and Hata, p. 20.

INTRODUCTION

KRAS is one of the most frequently mutated oncogenes in cancer; however, efforts to directly target KRAS have been largely unsuccessful due to its high affinity for GTP/GDP and the lack of a clear binding pocket (1–4). More recently, compounds were identified that covalently bind to KRAS^{G12C} at the cysteine 12 residue, lock the protein in its inactive GDP-bound conformation, inhibit KRAS-dependent signaling, and elicit antitumor responses in tumor models (5–7). Advances on early findings demonstrated that the binding pocket under the switch II region was exploitable for drug discovery, culminating in the identification of more potent KRAS^{G12C} inhibitors with improved physiochemical properties that are now entering clinical trials. The identification of KRAS^{G12C} inhibitors provides a renewed opportunity to develop a more comprehensive understanding of the role of KRAS as a driver oncogene and to explore the clinical utility of direct KRAS inhibition.

KRAS^{G12C} mutations are present in lung and colon adenocarcinomas as well as smaller fractions of other cancers. The genetic context of *KRAS*^{G12C} alteration can vary significantly among tumors and is predicted to affect response to KRAS inhibition. *KRAS* mutations are often enriched in tumors due to amplification of mutant or loss of wild-type allele (8, 9). In addition, *KRAS* mutations often co-occur with other key genetic alterations including *TP53* and *CDKN2A* in multiple cancers, *KEAP1* and/or *STK11* in lung adenocarcinoma, or *APC* and *PIK3CA* in colon cancer (3, 8–12). Whether differences in *KRAS*-mutant allele fraction or co-occurrence with other mutations influence response to KRAS blockade is not yet well understood. In addition, due to the critical importance of the RAS pathway in normal cellular function, there is extensive pathway isoform redundancy and a comprehensive regulatory network in normal cells to ensure tight control of temporal pathway signaling. RAS pathway negative feedback signaling is mediated by ERK1/2 and receptor tyrosine kinases (RTK) as well as by ERK pathway target genes including dual-specificity phosphatases (DUSP) and Sprouty (SPRY) proteins (13–17). One important clinically relevant example is provided by the reactivation of ERK signaling observed following treatment of *BRAF*^{V600E}-mutant cancers with selective BRAF inhibitors (18–20). The observed intertumoral heterogeneity and extensive feedback signaling network in KRAS-mutant cancers may necessitate strategies to more comprehensively block oncogenic signal transduction and deepen the antitumor response in concert with KRAS blockade (15, 21, 22).

Potential strategies to augment the response to KRAS^{G12C} inhibitor treatment are evident at multiple nodes of the signaling pathway regulatory machinery. RAS proteins are small GTPases that normally cycle between an active, GTP-bound

[1]Mirati Therapeutics, Inc., San Diego, California. [2]Array BioPharma Inc., Boulder, Colorado. [3]Memorial Sloan Kettering Cancer Center, New York, New York. [4]Monoceros Biosystems LLC, San Diego, California. [5]George Mason University, Manassas, Virginia. [6]Dana-Farber Cancer Institute, Boston, Massachusetts. [7]Henry Ford Medical Center, Detroit, Michigan. [8]Sarah Cannon Research Institute Tennessee Oncology, Nashville, Tennessee. [9]University of California, Irvine, Chao Family Comprehensive Cancer Center, Orange, California. [10]START Center for Cancer Care, San Antonio, Texas.

Note: Supplementary data for this article are available at Cancer Discovery Online (http://cancerdiscovery.aacrjournals.org/).

Corresponding Author: James G. Christensen, 9393 Towne Center Drive, Suite 200, San Diego, CA 92121. Phone: 858-332-3426; Fax: 858-597-1009; E-mail: christensenj@mirati.com

Cancer Discov 2020;10:54–71

doi: 10.1158/2159-8290.CD-19-1167

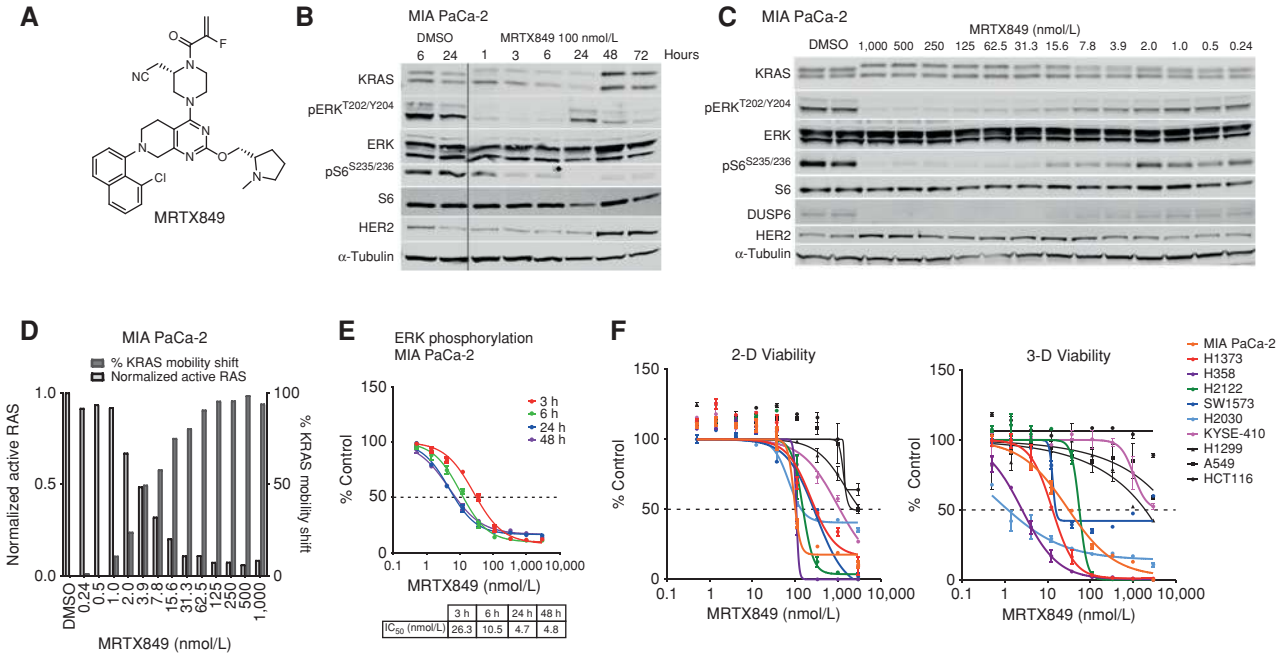

Figure 1. MRTX849 is a potent, covalent KRAS^{G12C} inhibitor *in vitro*. **A,** Structure of MRTX849. **B,** Immunoblot protein Western blot analyses of KRAS pathway targets in MIA PaCa-2 cells treated from 1 hours to 72 hours with MRTX849 at 100 nmol/L. **C,** Immunoblot protein Western blot analyses of KRAS pathway targets in MIA PaCa-2 cells treated for 24 hours with MRTX849 over a 13-point dose response. **D,** Left *y*-axis shows active RAS ELISA assay to determine the reduction in RAS-GTP abundance following MRTX849 treatment in MIA PaCa-2 cells for 24 hours. The vehicle value was normalized to 1 by dividing all average values by the vehicle value. Right *y*-axis shows quantitation of KRAS band shift by MRTX849 treatment in MIA PaCa-2 cells for 24 hours as assessed by Western blot and densitometry. **E,** In-cell Western blot assay to evaluate modulation of pERK in MIA PaCa-2 cells grown in standard tissue-culture conditions treated with MRTX849 over a time course. **F,** CellTiter-Glo assay to evaluate cell viability performed on seven *KRAS*^{G12C}-mutant cell lines and three non-*KRAS*^{G12C}-mutant cell lines grown in 2-D tissue-culture conditions in a 3-day assay (left plot) or 3-D conditions using 96-well, ULA plates in a 12-day assay (right plot).

state and an inactive, GDP-bound state. RAS proteins are loaded with GTP through guanine nucleotide exchange factors (e.g., SOS1) which are activated by upstream RTKs, triggering subsequent interaction with effector proteins that activate RAS-dependent signaling. RAS proteins hydrolyze GTP to GDP through their intrinsic GTPase activity, which is dramatically enhanced by GTPase-activating proteins (GAP). Mutations at codons 12 and 13 in RAS proteins impair GAP-stimulated GTP hydrolysis, leaving RAS predominantly in the GTP-bound, active state.

Potent covalent KRAS^{G12C} inhibitors described to date bind only GDP-bound KRAS (5–7). Although codon 12 and 13 mutations decrease the fraction of GDP-bound KRAS, recent biochemical analyses revealed that KRAS^{G12C} exhibits the highest intrinsic GTP hydrolysis rate and highest nucleotide exchange rate among KRAS mutants (23). Furthermore, the nucleotide-bound state of KRAS^{G12C} can be shifted toward the GDP-bound state by pharmacologically modulating upstream signaling with RTK inhibitors that increase the activity of KRAS^{G12C} inhibitors (7, 22, 24). Likewise, SHP2 is a phosphatase that positively transduces RTK signaling to KRAS. Accordingly, SHP2 inhibitors are active in cancers driven by KRAS mutations that are dependent on nucleotide cycling, including KRAS^{G12C} (25–27).

MRTX849 is among the first KRAS^{G12C} inhibitors to advance to clinical trials. The comprehensive and durable inhibition of KRAS^{G12C} by MRTX849 provides a unique opportunity to understand the extent to which KRAS functions as an oncogenic driver. In addition, the observation that the response to blockade of KRAS is markedly different *in vitro* and *in vivo* indicates that evaluation of the consequences of KRAS blockade in *in vivo* model systems is critical to understand the role of KRAS-driven tumor progression. The demonstration of partial responses in patients with lung and colon adenocarcinomas treated with MRTX849 in clinical trials indicates that results observed in tumor models extend to *KRAS*^{G12C}-positive human cancers. Our comprehensive molecular characterization of multiple tumor models at baseline and during response to KRAS inhibition has provided further insight toward the contextual role of KRAS mutation in the setting of genetic and tumoral heterogeneity. Finally, further interrogation of these genetic alterations and signaling pathways utilizing functional genomics strategies including CRISPR and combination approaches uncovered regulatory nodes that sensitize tumors to KRAS inhibition when cotargeted.

RESULTS

MRTX849 Is a Potent and Selective Inhibitor of KRAS^{G12C}, KRAS-Dependent Signal Transduction, and Cell Viability *In Vitro*

A structure-based drug design approach, including optimization for favorable drug-like properties, led to the

discovery of MRTX849 as a potent, covalent KRAS^{G12C} inhibitor (Fig. 1A; Supplementary Table S1). An LC/MS-based KRAS^{G12C} protein modification assay revealed that MRTX849 demonstrated much greater modification of KRAS^{G12C} when preloaded with GDP compared with GTP (Supplementary Table S2), supporting that MRTX849 binds to and stabilizes the inactive GDP-bound form of KRAS^{G12C}. Indeed, introducing a comutation that impairs the GTPase activity of KRAS^{G12C} (24) attenuated the inhibitory activity of MRTX1257, a close analogue of MRTX849 (Supplementary Fig. S1A). Secondary mutations that modulate the nucleotide exchange function of KRAS^{G12C} also affected inhibition by MRTX1257, supporting that the MRTX compound series is dependent on KRAS^{G12C} nucleotide cycling.

We next determined the cellular activity of MRTX849 utilizing the *KRAS*^{G12C}-mutant H358 lung and MIA PaCa-2 pancreatic cancer cell lines. In both models, MRTX849 demonstrated an upward electrophoretic mobility shift of KRAS^{G12C} protein band migration by immunoblot, indicative of covalent modification of KRAS^{G12C}. A maximal mobility shift was observed by 1 hour, was maintained through 72 hours (Fig 1B; Supplementary Fig. S1B), and was evident at concentrations as low as 2 nmol/L with near-maximal modification observed at 15.6 nmol/L (Fig. 1C; Supplementary Fig. S1C). Comparable inhibition of active RAS was observed as determined by a RAF RAS-binding domain capture ELISA assay (Fig. 1D; 1D). MRTX849 also inhibited KRAS-dependent signaling targets including ERK1/2 phosphorylation (pERK; Thr^{202}/Tyr^{204} ERK1), S6 phosphorylation (pS6; RSK-dependent Ser$^{235/236}$), and expression of the ERK-regulated DUSP6, each with IC_{50} values in the single-digit nanomolar range in both cell lines (Fig. 1B and C; Supplementary Fig. S1B and S1C). The evaluation of pERK over a time course of 48 hours indicated maximal inhibition was observed at 24 hours (Fig. 1E; Supplementary Fig. S1E). Treatment with the des-acrylamide version of MRTX849, which is unable to covalently bind to KRAS^{G12C}, did not demonstrate significant inhibition of ERK phosphorylation (Supplementary Fig. S1F). The H358 cell line was selected for determination of MRTX849 cysteine selectivity utilizing an LC/MS-based proteomics approach able to detect approximately 6,000 cysteine-containing peptides. After treatment for 3 hours, decreased KRAS^{G12C} Cys12-free peptide was detected with treated-to-control ratios of 0.029 and 0.008 determined at 1 and 10 μmol/L, respectively, indicating near-complete engagement of the intended target (Supplementary Table S3). In contrast, the only other peptides identified were from lysine-tRNA ligase (KARS) at Cys209 near the detection limit, indicating a high degree of selectivity toward KRAS^{CYS12}.

To evaluate the breadth of MRTX849 activity, its effect on cell viability was determined across a panel of 17 KRAS^{G12C}-mutant and 3 non–KRAS^{G12C}-mutant cancer cell lines using 2-D (3-day, adherent cells) and 3-D (12-day, spheroids) cell-growth conditions. MRTX849 potently inhibited cell growth in the vast majority of KRAS^{G12C}-mutant cell lines with IC_{50} values ranging between 10 and 973 nmol/L in the 2-D format and between 0.2 and 1,042 nmol/L in the 3-D format (Supplementary Table S4; Fig. 1F). In agreement with prior KRAS^{G12C} inhibitor studies (5), MRTX849 demonstrated improved potency in the 3-D assay format, as all but one KRAS^{G12C}-mutant cell line exhibited an IC_{50} value below 100 nmol/L. Although MRTX849 was broadly effective in inhibiting viability of KRAS^{G12C}-mutant cell lines, IC_{50} values varied across the cell panel by 100-fold, suggesting a differential degree of sensitivity to treatment. All three non–*KRAS*^{G12C}-mutant cell lines tested demonstrated IC_{50} values greater than 1 μmol/L in 2-D conditions and greater than 3 μmol/L in 3-D conditions, suggesting the effect of MRTX849 on cell viability was dependent on the presence of KRAS^{G12C}.

To determine whether the difference in sensitivity across the cell panel correlated with the ability of MRTX849 to bind to KRAS or inhibit KRAS-dependent signal transduction, seven KRAS^{G12C}-mutant cancer cell lines were selected from the panel for further evaluation. In each cell line, MRTX849 demonstrated a very similar concentration-dependent electrophoretic mobility shift (IC_{50}) for KRAS^{G12C} protein migration, suggesting that the ability to bind to and modify KRAS^{G12C} does not readily account for differences in response in viability studies (Fig. 1B and C; Supplementary Figs. S1B and S1C and S2A and S2B). The effect of MRTX849 on selected phosphoproteins implicated in mediating KRAS-dependent signaling was also evaluated across the cell panel by immunoblot and/or reverse-phase protein array (RPPA) following treatment for 6 or 24 hours. Notably, the concentration–response relationship and maximal effect of MRTX849 on inhibition of ERK and S6$^{S235/236}$ phosphorylation varied across the cell panel (Supplementary Fig. S2A and S2C; Supplementary Table S7). MRTX849 demonstrated only partial inhibition of pERK in KYSE-410 and SW1573 cells and a minimal effect on pS6$^{S235/236}$ in SW1573, H2030, and KYSE-410 cells (Supplementary Fig. S2A and S2C). Each of these cell lines were among those that exhibited a submaximal response to MRTX849 in both 2-D and 3-D viability assays (Fig. 1F). Although KRAS is implicated in mediating signal transduction through the PI3K and mTOR pathways, there was minimal evidence of a significant and/or durable effect of MRTX849 on AKT (S473, T308) or 4E-BP1 (T37/T46, S65, T70) phosphorylation at any time point in any cell lines evaluated (Supplementary Fig. S2D). However, MRTX849 demonstrated concentration-dependent partial inhibition of the mTOR-dependent signaling targets p70 S6 kinase (T412) and/or pS6 (S240/44) in the H358, MIA PaCa-2, H2122, and H1373 cell lines, each of which exhibited a maximal response to treatment. Together, these data suggest that maximizing inhibition of KRAS-dependent ERK and S6 signaling may be required to elicit a robust response in tumor-cell viability assays.

MRTX849 Treatment *In Vivo* Leads to Dose-Dependent KRAS^{G12C} Modification, KRAS Pathway Inhibition, and Antitumor Efficacy

Studies were conducted to evaluate MRTX849 antitumor activity along with its pharmacokinetic and pharmacodynamic properties *in vivo*, both to understand the clinical utility of this agent and to provide insight toward response to treatment. MRTX849 demonstrated moderate plasma clearance and prolonged half-life following oral administration

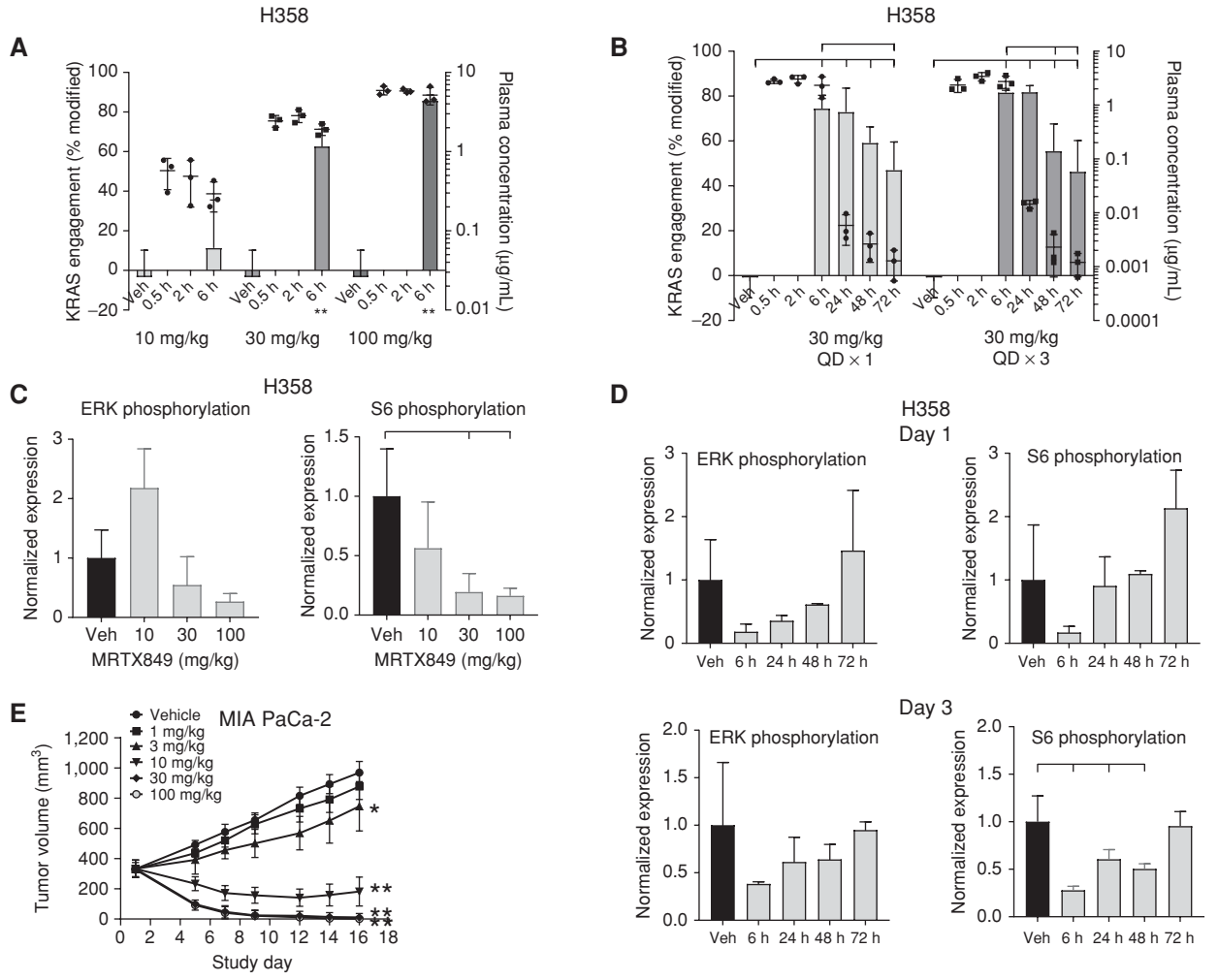

Figure 2. MRTX849 modifies KRAS^{G12C} and inhibits KRAS signaling and tumor growth *in vivo*. **A,** MRTX849 was administered orally as a single dose to mice bearing established H358 xenografts (average tumor volume ~350 mm^3) at 10, 30, and 100 mg/kg. KRAS modification and MRTX849 plasma concentration data from $n = 3$ mice are shown as mean ± SD. KRAS^{G12C} modification was statistically significant versus vehicle control using the two-tailed Student *t* test. **, $P < 0.01$. **B,** MRTX849 was administered orally as a single dose or daily (QD) for 3 days to mice bearing established H358 xenografts (average tumor volume ~350 mm^3) at 30 mg/kg. Plasma was collected at 0.5, 2, 6, 24, 48, and 72 hours after administration of the last dose, and tumors were collected at 6, 24, 48, and 72 hours after dose. KRAS^{G12C} modification and MRTX849 plasma concentration data are shown from $n = 3$ mice as mean ± SD. Induction of modified KRAS^{G12C} protein at all time points was determined to be statistically significant versus vehicle control using two-way ANOVA. In addition, induction of modified KRAS^{G12C} protein at 72 hours in day 1 samples and 48 and 72 hours in day 3 samples was statistically significant versus the 6-hour time point. Brackets indicate $P < 0.05$ as compared with left-most sample. **C,** MRTX849 was administered as in **A**. Tumors were collected 6 hours after dose, and total and phosphorylated ERK1/2 and total and phosphorylated S6 were analyzed by immunoblot and quantified by densitometric analysis. Relative fluorescence intensity of pERK1/2 and pS6 was normalized by dividing pERK1/2 and pS6 by total ERK1/2 and total S6, respectively. Vehicle-treated tumors were normalized to 1 by dividing all average values by the vehicle value. Average pERK1/2 and pS6 values were divided by the average value in vehicle-treated tumors. Data shown represent the average of 2 to 3 tumors per treatment group plus SD. Reduction of pS6 relative fluorescence intensity was determined to be statistically significant versus vehicle control using the two-tailed Student *t* test. Brackets indicate $P < 0.05$ compared with left-most sample. **D,** MRTX849 was administered as in **B**. Tumors were collected at 6, 24, 48, or 72 hours after administration of the last dose, and total and phosphorylated ERK1/2 and total and phosphorylated S6 were analyzed as in **C**. Data shown represent the average of 3 to 4 tumors per treatment group plus SD. Reduction of pS6 relative fluorescence intensity on day 3 was determined to be statistically significant versus vehicle control using two-way ANOVA. Brackets indicate $P < 0.05$ compared with left-most sample. **E,** MRTX849 was administered via daily oral gavage at the doses indicated to mice bearing established MIA PaCa-2 xenografts. Dosing was initiated when tumors were approximately 350 to 400 mm^3. MRTX849 was administered to mice daily until day 16. Data are shown as mean tumor volume ± SEM. Tumor volumes at day 16 were determined to be statistically significant versus vehicle control via two-tailed Student *t* test. **, $P < 0.01$; *, $P < 0.05$.

(Supplementary Table S1; Supplementary Fig. S3). To evaluate the pharmacodynamic response to MRTX849 and to correlate drug exposure with target inhibition, MRTX849 was administered via oral gavage over a range of dose levels to H358 xenograft–bearing mice, and plasma and tumors were collected at defined time points. The fraction of covalently modified KRAS^{G12C} protein was proportional to the plasma concentration of MRTX849 (Fig. 2A). When evaluated over time after a single oral dose at 30 mg/kg, the modified fraction of KRAS^{G12C} was 74% at 6 hours after dose

and gradually decreased to 47% by 72 hours (Fig. 2B). This extended pharmacodynamic effect, despite declining levels of MRTX849 in plasma, was consistent with the irreversible inhibition of KRAS^{G12C} by MRTX849 and the relatively long half-life for the KRAS^{G12C} protein (~24–48 hours; Supplementary Table S5). The modification of KRAS^{G12C} was maximized after repeated daily dosing for 3 days at 30 mg/kg (Fig. 2B), and higher dose levels did not demonstrate additional KRAS^{G12C} modification in multiple tumor models (data not shown). The maximum level of modification of approximately 80%, despite increasing dose and plasma levels of MRTX849, suggests that accurate measurement of complete inhibition of KRAS^{G12C} utilizing LC/MS may not be attainable, potentially due to a pool of active, noncycling, or unfolded KRAS^{G12C} protein in tumors. Together, these studies demonstrated a dose-dependent increase in covalent modification of KRAS^{G12C} by MRTX849 and that the majority of targetable KRAS was covalently modified by MRTX849 over a repeated administration schedule at dose levels at or exceeding 30 mg/kg.

To evaluate the effect of MRTX849 on KRAS-dependent signal transduction *in vivo*, a single dose of MRTX849 at 10, 30, or 100 mg/kg was administered to H358 tumor–bearing mice. Dose-dependent inhibition of ERK1/2 and pS6$^{S235/36}$ phosphorylation was observed at 6 hours after dose based on immunoblot and densitometric analysis (Fig. 2C). MRTX849 also demonstrated marked inhibition of ERK1/2 and S6$^{S235/36}$ phosphorylation after one or three daily doses at 6 or 24 hours, and levels gradually recovered by 72 hours after the final dose (Fig. 2D). pERK1/2 and pS6$^{S235/36}$ were further evaluated in formalin-fixed, paraffin-embedded sections from vehicle-treated and MRTX849-treated xenografts in four tumor models utilizing IHC methods coupled with image analysis algorithms. These studies demonstrated increased pERK1/2 and pS6 in nontumor/stromal cells following MRTX849 administration, indicating that immunoblotting studies with bulk tumor lysate likely underrepresent the degree of pathway inhibition in tumor cells, whereas IHC-based evaluation may more accurately reflect both the degree and spatial impact of pathway inhibition. Maximal inhibition was observed for both ERK and S6$^{S235/36}$ phosphorylation after a single dose at the 6-hour time point, with a rebound in signaling evident 24 hours after single dose in each model (Supplementary Fig. S4). Marked inhibition of ERK phosphorylation was observed at 6 hours after administration, with 89%, 94%, and 94% inhibition observed compared with vehicle controls in MIA PaCa-2, H1373, and H2122 tumors, respectively (H358 pERK not quantifiable). This indicates that dose levels at or exceeding 30 mg/kg dose maximized inhibition of ERK phosphorylation in multiple models (Supplementary Fig. S4A and S4B). Inhibition of S6 phosphorylation at 6 hours was more variable, with percent inhibition values of 76%, 50%, 86%, and 56% observed in MIA PaCa-2, H1373, H358, and H2122 tumors, respectively (Supplementary Fig. S4B). Together, these data indicate that consistent acute (6 hours) inhibition of KRAS-dependent ERK phosphorylation was maximized in all evaluated models, whereas inhibition of S6$^{S235/36}$ was more variable, presumably due to varying degrees of KRAS-independent activation of this pathway in different tumor models.

MIA PaCa-2 and H358 were selected as MRTX849-responsive tumor models, thereby enabling a high-resolution understanding of dose–response relationships. Significant, dose-dependent, antitumor activity was observed at the 3, 10, 30, and 100 mg/kg dose levels in the MIA PaCa-2 model (Fig. 2E). Evidence of rapid tumor regression was observed at the earliest post-treatment tumor measurement, and animals in the 30 and 100 mg/kg cohorts exhibited evidence of a complete response at study day 15. Dosing was stopped at study day 16, and all 4 mice in the 100 mg/kg cohort and 2 of 7 mice in the 30 mg/kg cohort remained tumor-free through study day 70 (Supplementary Fig. S5A). In a second MIA PaCa-2 study, dose-dependent antitumor efficacy was observed at the 5, 10, and 20 mg/kg dose levels, and 2 of 5 mice at the 20 mg/kg dose level exhibited complete tumor regression (Supplementary Fig. S5B). Significant dose-dependent antitumor efficacy was also observed in the H358 model, including 61% and 79% tumor regression at the 30 and 100 mg/kg dose levels, respectively, at day 22 (Supplementary Fig. S5C). MRTX849 was well tolerated, and no effect on body weight was observed at all dose levels evaluated (Supplementary Fig. S5D). These studies indicated that MRTX849 demonstrated dose-dependent antitumor efficacy over a well-tolerated dose range and that the maximally efficacious dose of MRTX849 is between 30 and 100 mg/kg/day.

MRTX849 Demonstrates Broad-Spectrum Tumor Regression in KRAS^{G12C} Cell Line and Patient-Derived Xenograft Models

To evaluate the breadth of antitumor activity across genetically and histologically heterogeneous KRAS^{G12C}-mutant cancer models, MRTX849 was evaluated at a fixed dose of 100 mg/kg/day (a dose projected to demonstrate near-maximal target inhibition in most models) in a panel of human *KRAS*^{G12C}-mutant cell line–derived xenograft (CDX) and patient-derived xenograft (PDX) models. MRTX849 demonstrated tumor regression exceeding 30% volume reduction from baseline in 17 of 26 models (65%) at approximately 3 weeks of treatment (Fig. 3A; Supplementary Table S6). By comparison, MRTX849 did not exhibit significant antitumor activity at 100 mg/kg in three non–*KRAS*^{G12C}-mutant models (Fig. 3A; Supplementary Table S6). Together, these results indicate that *KRAS*^{G12C}-mutant tumors are broadly dependent upon mutant KRAS for tumor-cell growth and survival and that MRTX849 elicits antitumor activity through a KRAS^{G12C}-dependent mechanism.

Although MRTX849 exhibited marked antitumor responses in the majority of models tested, a response pattern ranging from delayed tumor growth to complete regression was observed across the xenograft panel. The response to treatment was categorized as sensitive, partially sensitive, or treatment refractory (Fig. 3B). Rank order and Pearson statistical analyses were performed to evaluate the correlation between *in vitro* potency (IC_{50} in 2-D or 3-D viability assays) and antitumor response *in vivo* (% regression or progression on day 22), and a significant correlation between response in cell lines compared with tumor models was not observed (Supplementary Fig. S6A and S6B). Thus, we focused on a comprehensive analysis of correlates with

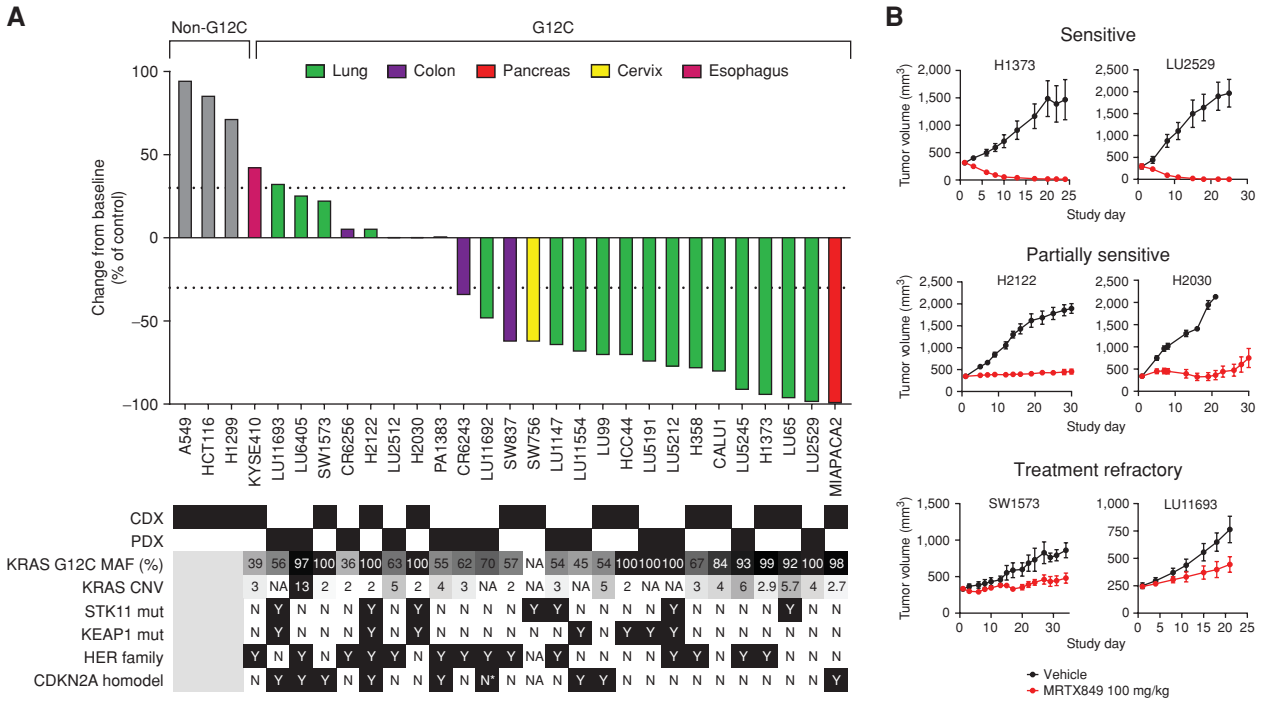

Figure 3. Antitumor activity of MRTX849 in *KRAS*^{G12C}-mutant and non-*KRAS*^{G12C}-mutant human tumor xenograft models. **A,** MRTX849 was administered via oral gavage at 100 mg/kg every day to mice bearing the CDX or PDX model indicated. Dosing was initiated when tumors were, on average, approximately 250 to 400 mm^3. MRTX849 was formulated as a free base and resuspended as a solution in 10% Captisol and 50 mmol/L citrate buffer, pH 5.0. The percent change from baseline control was calculated at days 19 to 22 for most models. Statistical significance was determined for each model and is shown in Supplementary Table S6. Status of mutations and alterations in key genes is shown below each model. MAF (%), percent *KRAS*^{G12C}-mutant allele fraction by RNA-seq; CNV, copy-number variation; * denotes very high CDK4 expression by RNA-seq and possible amplification. HER family status was determined by averaging *EGFR*, *ERBB2*, and *ERBB3* RNA-seq expression for CDX (CCLE) or PDX (Crown huBase) models. Positive HER family calls denote greater than the median expression of the models tested. CDX and PDX model HER family calls were determined independently. **B,** Tumor-growth inhibition plots from representative xenograft models that were categorized as sensitive, partially sensitive, or treatment refractory.

MRTX849 tumor response *in vivo*, including tumor histology, co-occurring genetic alterations, as well as baseline or drug-induced changes in expression of KRAS-related genes [RNA sequencing (RNA-seq)] and/or protein signaling networks (RPPA in 18 models, ref. 28; Supplementary Fig. S7). No individual genetic alteration, including but not limited to *KRAS*-mutant allele frequency, *TP53, STK11*, or *CDKN2A,* predicted the antitumor activity of MRTX849. Interestingly, baseline gene and/or protein expression of selected members of the HER family of RTKs and of regulators of early cell-cycle transition did exhibit a trend with the degree of antitumor response, suggesting these pathways may influence the response to KRAS inhibitors (Supplementary Fig. S7A). Together, these data indicate that there are no individual binary biomarkers that clearly predict therapeutic response and that the molecular complexity and heterogeneity present in distinct KRAS-mutated tumors may contribute to the response to target blockade.

MRTX849 Antitumor Activity Translates to RECIST Responses in Patients with Cancer

A 45-year-old female former smoker diagnosed with stage IV lung adenocarcinoma and refractory to multiple lines of therapy including carboplatin/pemetrexed/pembrolizumab, docetaxel, and investigational treatment with binimetinib and palbociclib was enrolled onto the MRTX849-001 phase Ib clinical trial with two bilateral lung lesions and mediastinal lymph node as target lesions. Targeted next-generation sequencing (NGS) demonstrated a *KRAS*^{G12C} mutation (c.34G>T). In addition, loss-of-function *KEAP1* (K97M) and *STK11* (E223*) mutations were detected and are predicted to be deleterious to their respective proteins. The patient was administered MRTX849 (600 mg twice a day) and had marked clinical improvement within 2 weeks, including complete resolution of baseline cough and oxygen dependency. A RECIST-defined partial response of 33% reduction of target lesions was observed at cycle 3 day 1 (45 days), and the patient continues on study (Fig. 4A).

A 47-year-old female never-smoker with metastatic adenocarcinoma of the left colon who exhibited progressive disease after receiving multiple lines of systemic therapy, including FOLFOX plus bevacizumab, single-agent capecitabine, FOLFIRI plus bevacizumab, and an investigational antibody–drug conjugate, was enrolled into the MRTX849-001 phase Ib clinical trial. This patient had extensive metastases involving the liver, peritoneum, ovaries, and lymph nodes. Targeted NGS identified a *KRAS*^{G12C} mutation. The patient was administered MRTX849 (600 mg twice a day) and demonstrated marked clinical improvement within 3 weeks and a visible

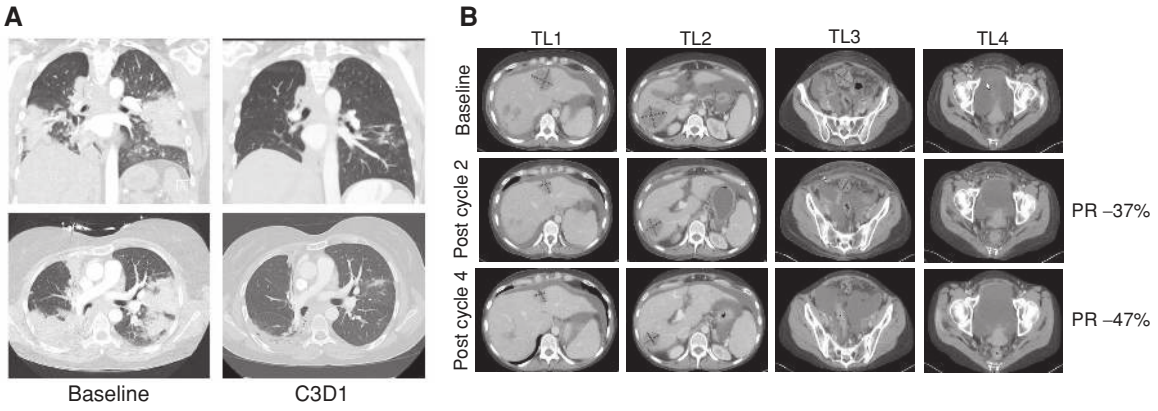

Figure 4. Activity of MRTX849 in patients with lung and colon cancers. **A,** Pretreatment and 6-week scans of a heavily pretreated patient with a *KRAS*^{G12C} mutation–positive lung adenocarcinoma indicating 33% reduction of target lesions. Patient continues on study. The top plots show a coronal view, and bottom plots an axial view of CT chest images prior to MRTX849 treatment (left) and after two cycles of MRTX849 treatment (right). **B,** Baseline, 6-week (Cycle 2), and 12-week (Cycle 4) scans of a patient with a *KRAS*^{G12C} mutation–positive colon adenocarcinoma. Partial response (PR) was confirmed at Cycle 4, and patient continues on study. Four lesions (TL1–4) are shown with axial views of CT images prior to MRTX849 treatment (top), after two cycles of MRTX849 treatment (center), and after four cycles of MRTX849 treatment (bottom).

decrease in size of her umbilical Sister Mary Joseph nodule. Her carcinoembryonic antigen levels decreased from 77 ng/mL at baseline to 11 ng/mL at cycle 2 day 1 and 3 ng/mL by cycle 3 day 1 (normal range, 0–5 ng/mL). A RECIST-defined partial response with a 37% reduction of target lesions and complete response of a nontarget lesion was observed at cycle 3 day 1 (day 42). Confirmatory CT scans were conducted at cycle 5, day 1 (day 84) and indicated a confirmed RECIST partial response with further reduction of target lesions at –47% from baseline (Fig. 4B). The patient remains on treatment through Cycle 6.

Temporal Effects of MRTX849 on KRAS-Dependent Signaling and Feedback Pathways and Relationship to Antitumor Activity Following Repeat Dosing in Xenograft Models

A comprehensive analysis was conducted to evaluate MRTX849-induced temporal molecular changes to further interrogate mechanisms of drug response across sensitive and partially sensitive models. To evaluate temporal changes in global gene expression, xenograft-bearing mice were administered vehicle or 100 mg/kg MRTX849, and RNA-seq was performed on tumors at 6 and 24 hours after treatment. Gene expression was evaluated at day 1 and day 5 for the sensitive models MIA PaCa-2 and H1373 to ensure sufficient tissue availability from regressing tumors, or at day 7 in the partially sensitive models H358, H2122, and H2030 to coordinate with tumor stasis plateau. The top differentially expressed gene set enrichment analysis (GSEA) hallmark gene sets, regardless of tumor response, in all five models were several KRAS-annotated gene sets confirming MRTX849 selectively inhibits multiple genes directly related to KRAS signaling. MYC, mTOR, cell cycle, and apoptosis/BCL2 pathway gene sets were also strongly differentially expressed, confirming MRTX849 broadly affected multiple well-established, KRAS-regulated pathways, several of which have proved difficult to directly inhibit with previous targeted therapies (Fig. 5A and B; Supplementary Fig. S8A–S8D). The marked impact of MRTX849 on a large number of genes that regulate cell cycle and apoptosis provides further insight into molecular mechanisms which mediate its antitumor activity.

Targeted RNA-seq analysis was performed on genes implicated in the temporal regulation of external signaling inputs and feedback pathways which collectively temper signaling flux through the RAS–RAF–MEK–ERK MAP kinase (MAPK) pathway including *DUSP*, *SPRY*, and *PHLDA* family genes (13, 18). These MAPK pathway–negative regulators were each ranked among the most strongly decreased genes following MRTX849 treatment, providing evidence that ERK-dependent transcriptional output is blocked and that pathways involved in reactivation of RTK- and ERK-dependent signaling were activated (Fig. 5C; Supplementary Fig. S4A).

On the basis of the observation of dynamic changes in transcriptional programs linked to KRAS pathway reactivation, IHC plus quantitative imaging of tumor cell–specific pERK and pS6 was evaluated over a range of time points. In the sensitive MIA PaCa-2 and H1373 tumor models, treatment with MRTX849 (100 mg/kg) demonstrated ≥90% inhibition of ERK phosphorylation at 6 and 24 hours on both days 1 and 5 (Supplementary Fig. S4). In contrast, in the partially sensitive H358 and H2122 models, robust inhibition of ERK phosphorylation was observed at 6 hours after a single dose; however, marked recovery of ERK phosphorylation was observed at 24 hours after single dose and at both 6 and 24 hours following 7 days of repeat-dose administration. Because *DUSP*, *SPRY*, and *ETV* family transcripts remain downregulated through 5 to 7 days in all models, it is evident that other independent factors contribute to temporal reactivation of ERK (Fig. 5C). Similar to what was observed with single-dose administration, the effect of MRTX849 on pS6 was variable over time and did not track with the antitumor activity of MRTX849. Together, these

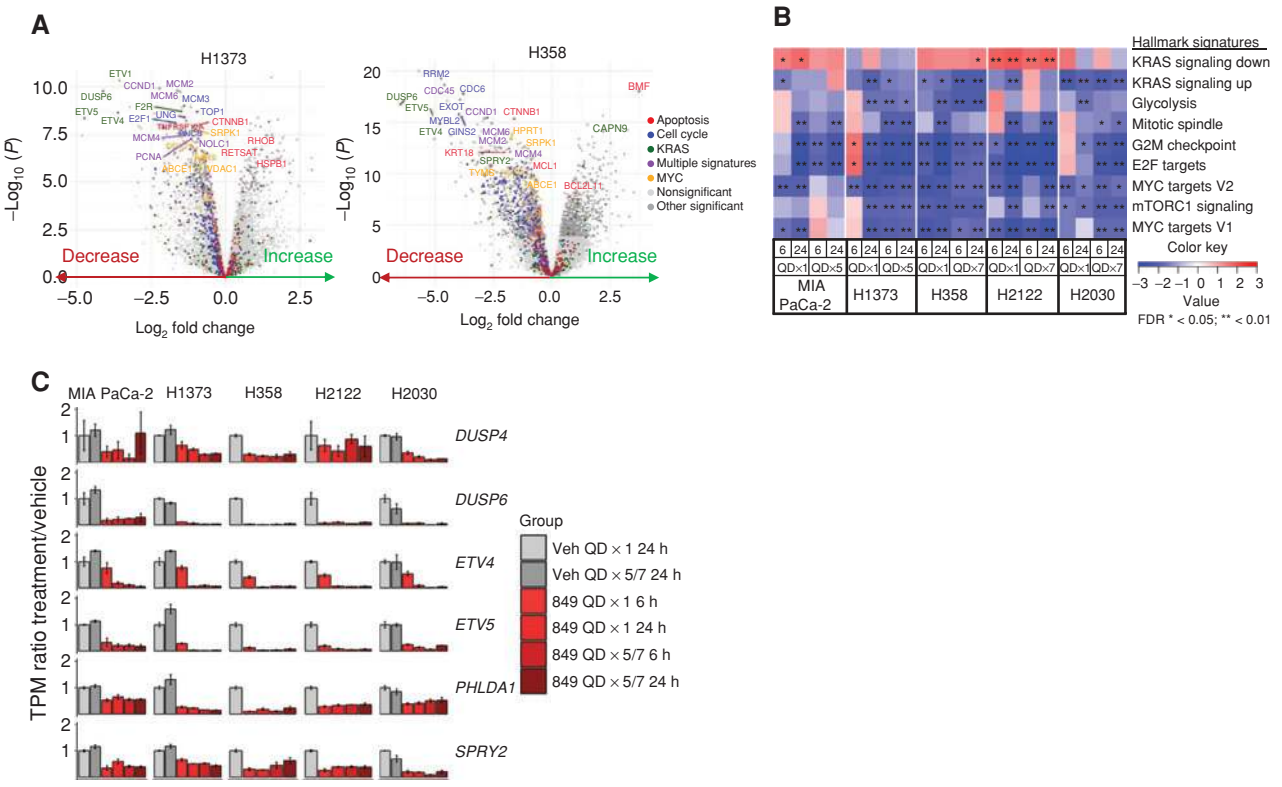

Figure 5. MRTX849 treatment *in vivo* regulates KRAS-dependent oncogenic signaling and feedback-inhibitory pathways. **A,** Volcano plots displaying differentially expressed genes in xenograft tumors 24 hours after oral administration of vehicle or 100 mg/kg MRTX849 in a representative MRTX849-sensitive (H1373) and MRTX849-partially sensitive (H358) model. Significance denoted in the legend ($P_{adj} < 0.01$). **B,** GSEA heat maps depicting hallmark signature pathways differentially regulated in at least one model 24 hours following oral administration of a single 100 mg/kg MRTX849 dose compared with vehicle. Normalized enrichment score shown in all models 6 or 24 hours after a single dose (QD × 1) or 5 (QD × 5) or 7 (QD × 7) days dosing. **C,** Genes that feedback-inhibit MAP kinase signaling are downregulated following MRTX849 treatment in all five cell line xenografts assessed by RNA-seq. TPM, Transcripts Per Kilobase Million.

results suggest that the extent and duration of inhibition of pERK may track with the magnitude of antitumor efficacy of KRAS^{G12C} inhibitors and that further evaluation of the role of S6 is required to understand if it plays a role in drug sensitivity.

The effect of MRTX849 on cell proliferation and apoptosis was characterized by IHC analysis of Ki-67 or cleaved caspase-3 after a single dose or repeat administration. The fraction of Ki-67–positive cells was significantly reduced in tumors after repeat administration in all four models tested, further supporting a broadly operative antiproliferative mechanism, independent of the magnitude of MRTX849 antitumor response (Supplementary Fig. S4). Induction of apoptosis as determined by cleaved caspase-3 immunostaining was also evident on day 1 of treatment (6 and/or 24 hours after treatment) in the sensitive H358, MIA PaCa-2, and H1373 models (79%–100% maximal regression) but not in the partially sensitive H2122 model (Supplementary Fig. S4). An expanded RPPA-based pathway analysis of several models also indicated a correlation between antitumor activity of MRTX849 and decreased survivin (statistically significant at days 5/7 in 7 models evaluated; Supplementary Fig. S7B) and a trend toward increased cleaved caspase-3 induction (day 1, $P = 0.08$, 16 models), supporting the induction of apoptosis as a key mediator of a cytoreductive antitumor response (Supplementary Fig. S7C). Interestingly, the magnitude of reduction of MYC and cyclin B1 protein levels at days 5/7 also closely correlated with MRTX849 antitumor activity, consistent with their roles as critical regulators of KRAS-mediated cell growth and survival pathways (Supplementary Fig. S7B). Collectively, these data support that durable inhibition of ERK activity and maximal inhibition of ERK-regulated outputs including MYC and E2F-mediated transcription are associated with induction of apoptosis and maximal response to MRTX849 treatment.

CRISPR/Cas9 Screen Identifies Vulnerabilities and Modifiers of Response to MRTX849 in *KRAS*^{G12C}-Mutant Cancer Cell Lines *In Vitro* and *In Vivo*

The correlative analysis of genomic or proteomic markers with response to MRTX849 in the defined panel of models provided only limited insight toward mechanism of therapeutic response or resistance. Therefore, we directly interrogated the role of selected genes in mediating therapeutic response utilizing a focused CRISPR/Cas9 knockout screen targeting approximately 400 genes including many genes involved in KRAS signaling. This was conducted in H358 and H2122 cells *in vitro* and in H2122 xenografts *in vivo* in

the presence and absence of MRTX849 treatment (Supplementary Fig. S9A–S9F). In MRTX849-anchored screens *in vitro*, single guide RNAs (sgRNA) that target RAS signaling pathway genes including *MYC, SHP2* (H2122), mTOR pathway (*MTOR* and *RPS6*), and cell-cycle genes (*CDK1, CDK2, CDK4/6,* and *RB1*) were identified to affect cell fitness. sgRNAs that target *KEAP1* and *CBL* were enriched in the H2122 model, demonstrating cell-specific genetic routes toward improved fitness through loss of classic tumor-suppressor genes, including in the context of MRTX849 treatment. *KRAS* sgRNA dropout was less pronounced in the MRTX849-treated cells compared with DMSO control–treated cells, as would be expected with redundant depletion of the drug target (Supplementary Fig. S9C and S9D). To evaluate whether a distinct KRAS dependence or modulation of MRTX849 therapeutic response was observed *in vitro* versus *in vivo*, xenograft-bearing mice bearing H2122 cells (~250 mm^3) transduced with the sgRNA library were orally administered vehicle or MRTX849 for 2 weeks (Supplementary Fig. S9A, S9E, and S9F). In MRTX849-treated xenografts, sgRNAs targeting cell cycle, *SHP2, MYC,* and mTOR pathway genes remained among the top depleted sgRNAs, demonstrating that inhibition of these targets *in vivo*, in the context of KRAS inhibition, leads to further tumor-growth inhibition over and above the effects of KRAS inhibition alone (Supplementary Fig. S9E and S9F). sgRNAs targeting the tumor suppressor *KEAP1* were enriched in MRTX849-treated xenografts, suggesting loss of *KEAP1* may represent a mechanism of intrinsic or acquired resistance. Interestingly, *NRAS* was one of the top enriched genes in the vehicle-treated xenografts, suggesting *NRAS* functions as a tumor suppressor in this context; however, enrichment was not as pronounced in the MRTX849-treated xenografts, suggesting NRAS may compensate for KRAS in the context of KRAS inhibition (Supplementary Fig. S9F). Collectively, these data demonstrate the importance of selected proteins that regulate RTK- and RAS-dependent signaling and cell-cycle transition in mediating the oncogenic effects of mutant KRAS, and also provide a catalog of potentially druggable vulnerabilities that complement KRAS blockade.

Cancer Therapeutic Combination Screen to Identify Rational and Clinically Tractable Strategies to Address Feedback and Resistance Pathways

To further interrogate pathways that mediate the antitumor response to MRTX849 and to identify combinations capable of enhancing response to MRTX849, a combination screen was conducted *in vitro* using a focused library of small-molecule inhibitors across a panel of cell lines (Supplementary Fig. S10A and S10B; Supplementary Table S8). Approximately 70 compounds targeting relevant pathways (RTKs, MAPK/ERK, PI3K, mTOR, cell cycle) were tested in a 3- or 7-day viability assay, and synergistic combinations were identified and ranked. Multiple hits from this screen were then identified for additional evaluation in combination studies with MRTX849, including the HER family inhibitor afatinib, the CDK4/6 inhibitor palbociclib, the SHP2 inhibitor RMC-4550, and mTOR pathway inhibitors.

Combination Strategies That Target Upstream Signaling Pathways Implicated in Extrinsic Regulation of KRAS Nucleotide Cycling and Feedback/Bypass Pathways

MRTX849 in combination with HER family inhibitors synergistically inhibited tumor-cell viability in the majority of cell lines evaluated and were the top hit in the combination screen in *vitro* (Supplementary Fig. S10). Cell lines with the highest (top 50th percentile) average composite baseline RNA expression values of selected HER family members exhibited the highest synergy scores to these combinations (Supplementary Fig. S11A). Afatinib was selected as a prototype HER family inhibitor based on its broad *in vitro* combination activity. Combination studies were conducted with MRTX849 and afatinib in five tumor models that were partially sensitive or treatment refractory to single-agent MRTX849. The MRTX849 and afatinib combination demonstrated significantly greater antitumor efficacy compared with either single agent in all five models evaluated, including multiple models exhibiting complete or near-complete responses to the combination (Fig. 6A; Supplementary Fig. S11B).

To evaluate whether afatinib affected covalent modification of KRAS^{G12C} by MRTX849, partially sensitive H2122 cells were treated with increasing concentrations of MRTX849 alone or in the presence of afatinib (200 nmol/L, IC_{90}), and the mobility shift in KRAS protein was densitometrically determined from immunoblots. A clear shift in the concentration response to MRTX849 was apparent in the presence of afatinib, indicating that the combination increased the fraction of modified KRAS^{G12C} consistent with the putative role of HER family receptors in extrinsic regulation of KRAS^{G12C} GTP loading (Fig. 6B). The concentration–response relationship for inhibition of ERK phosphorylation was also clearly shifted in the presence of afatinib. To further evaluate the effect of the combination on KRAS-dependent signaling, four cell lines (H2030, H2122, H358, and KYSE-410) were treated with a range of MRTX849 concentrations in the presence or absence of afatinib for 6 or 24 hours, and key signaling molecules were evaluated by RPPA. Afatinib demonstrated clear inhibition of EGFR (pY1068) and HER2 (pY1248) activity and partial inhibition of ERK, AKT (S473), and p70S6K phosphorylation at both time points (Supplementary Fig. S11C). The effect of afatinib on S6 (S235/236, S240/244) and p90 RSK (S380) phosphorylation was variable and exhibited only minimal inhibition in most of the cell lines evaluated. The combination of afatinib and MRTX849 demonstrated markedly enhanced concentration-dependent inhibition and/or a greater magnitude of effect on ERK, RSK, p70 S6K, and S6 (S235/236) phosphorylation compared with MRTX849 alone at both 6 and 24 hours. Of note, neither afatinib nor MRTX849 alone inhibited S6 phosphorylation at the S240/244 site regulated by mTOR/S6K, whereas the combination demonstrated marked inhibition at 24 hours.

In vivo, the combination also exhibited a trend toward increased pERK and pS6 (S235/236) inhibition in the partially sensitive H2122 model in combination groups as determined by quantitation of immunostaining after 1- or 7-day

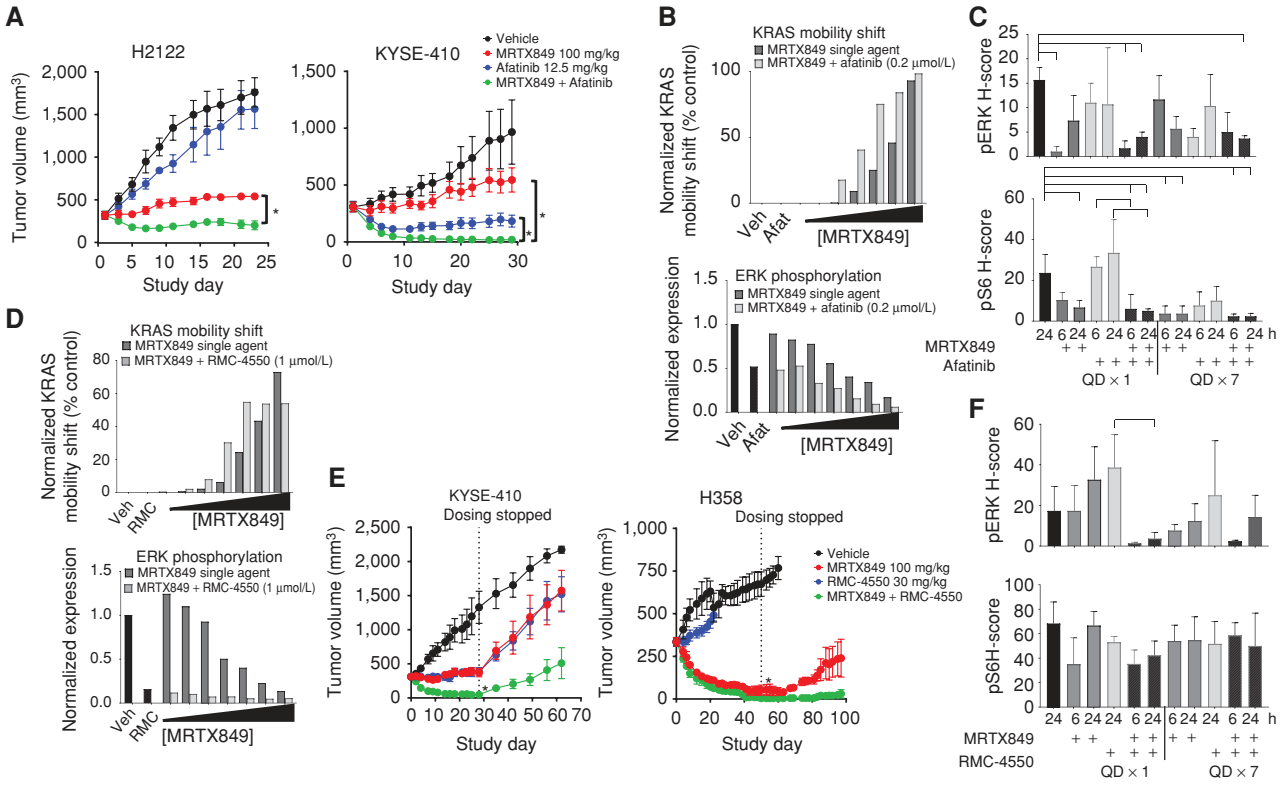

Figure 6. HER family and SHP2 inhibitor combinations further inhibit KRAS signaling and exhibit increased antitumor responses. **A,** MRTX849 at 100 mg/kg, afatinib at 12.5 mg/kg, or the combination was administered daily via oral gavage to mice bearing the H2122 or KYSE-410 cell line xenografts ($n = 5$). Combination treatment led to a statistically significant decrease in tumor growth compared with either single-agent treatment. *, $P_{adj} < 0.01$. **B,** Quantification of KRAS mobility shift and pERK in H2122 cells treated for 24 hours with MRTX849 (0.1–73 nmol/L), afatinib (200 nmol/L), or the combination assessed by Western blot densitometry. **C,** MRTX849 at 100 mg/kg, afatinib at 12.5 mg/kg, or the combination was administered once or daily for 7 days via oral gavage to mice bearing H2122 cell line xenografts ($n = 3$/group). Tumors were harvested at 6 and 24 hours following the final dose. Tumor sections were stained for pERK and pS6 via IHC methods. Quantitation of images shown by H-score in tumor tissue. Reduction of pERK or pS6 staining intensity was determined to be statistically significant relative to vehicle or either single agent using one-way ANOVA. Brackets indicate $P < 0.05$ compared with left-most sample. **D,** Quantitation of KRAS band shift and pERK after 24-hour treatment with MRTX849 (0.1–73 nmol/L), RMC-4550 (1 μmol/L), or the combination in H358 cells assessed by Western blot densitometry. **E,** MRTX849 at 100 mg/kg, RMC-4550 at 30 mg/kg, or the combination was administered daily via oral gavage to mice bearing the KYSE-410 or H358 cell line xenografts ($n = 5$/group). Combination treatment led to a statistically significant reduction in tumor growth compared with either single agent on the last day of dosing. *, $P_{adj} < 0.05$. **F,** MRTX849 at 100 mg/kg, RMC-4550 at 30 mg/kg, or the combination was administered via oral gavage to mice bearing KYSE-410 cell line xenografts ($n = 3$/group), and tumors were harvested at 6 and 24 hours post-dose. Tumor sections were stained with pERK or pS6 via IHC methods. Quantitation of images shown by H-score in tumor tissue. Reduction of pERK staining intensity was determined to be statistically significant relative to RMC-4550 alone using one-way ANOVA. Brackets indicate $P < 0.05$ compared with left-most sample.

administration (Fig. 6C). Similar results were observed in the MRTX849-refractory KYSE-410 model, and the combination also increased the number of apoptotic cells in this model (Supplementary Fig. S12A–S12C). Collectively, these data indicate that upstream baseline HER family activation may limit the ability of MRTX849 to achieve robust inhibition of the ERK and mTOR–S6 signaling pathways. Accordingly, the combination of afatinib and MRTX849 can limit feedback reactivation of ERK and demonstrate complementary inhibition of AKT–mTOR–S6 signaling, resulting in significantly improved antitumor activity.

SHP2 inhibition has been shown to inhibit the growth of cells that harbor $KRAS^{G12C}$ mutations, and this effect is likely mediated, in part, by decreasing KRAS GTP loading (25–27). To evaluate whether SHP2 inhibition enhanced covalent modification of $KRAS^{G12C}$ by MRTX849, H358 and H2122 cells were incubated with increasing MRTX849 concentrations with or without the SHP2 inhibitor RMC-4550. In both cell lines, cotreatment with RMC-4550 (1 μmol/L, IC_{90}) demonstrated a MRTX849 concentration-dependent increase in $KRAS^{G12C}$ protein modification and a concomitant decrease in ERK phosphorylation compared with MRTX849 alone (Fig. 6D; Supplementary Fig. S13A). RPPA analysis of KRAS-dependent signaling was conducted at 6 or 24 hours after treatment in three cell lines (H358, H2030, H2122) over a range of MRTX849 concentrations in the presence or absence of RMC-4550. RMC-4550 demonstrated robust inhibition of ERK phosphorylation and partial inhibition of p90 RSK (S380) and p70 S6K (T412) at both time points (Supplementary Fig. S13B). The combination of RMC-4550 and MRTX849 demonstrated incrementally increased concentration-dependent inhibition of ERK and RSK phosphorylation

in all cell lines at both 6 and 24 hours and markedly improved inhibition of S6 (S235/236) phosphorylation compared with MRTX849 alone in H2122 and H358 cells at 24 hours. In addition, the combination demonstrated near-complete inactivation of KRAS in MRTX849-refractory KYSE-410 xenografts as determined using an active RAS ELISA assay, and this was significant compared with single agents (Supplementary Fig. S13C). On the basis of these findings, combination studies were conducted with MRTX849 and RMC-4550 in six *KRAS*^{G12C}-mutated tumor models *in vivo,* and the combination demonstrated significantly greater antitumor efficacy compared with either single agent in 4 of 6 models evaluated (Fig. 6E; Supplementary Fig. S13D). Consistent with the *in vitro* data, the combination also demonstrated a significant decrease in ERK phosphorylation compared with either single agent in the KYSE-410 model as determined by quantitation of tumor-cell immunostaining on day 1 at 6 and 24 hours and day 7 at 6 hours after dose (Fig. 6F). Together, these data indicate that EGFR family and SHP2 blockade can augment the antitumor activity of KRAS^{G12C} inhibitors through enhancing covalent target modification and establishing a more comprehensive blockade of KRAS-dependent signaling.

Combinations That Inhibit Bypass Pathways Downstream of KRAS and Exhibit Increased Antitumor Activity in Xenograft Models

KRAS is implicated in regulation of the oncogenic S6 protein translation pathway through both ERK-dependent activation of RSK, which phosphorylates S6 at Ser$^{235/236}$, and cross-talk with the PI3K and mTOR pathway that additionally phosphorylates S6 at Ser$^{240/244}$ (29). However, the S6 pathway can also be activated independently of mutated KRAS in tumor cells through hyperactivated RTK signaling, PI3K activation, or *STK11* mutations, each of which converge on mTOR-mediated activation of S6. In the *in vitro* combination screen, mTOR inhibitors demonstrated synergy in a subset of evaluated cell lines (Supplementary Fig. S14A). To further evaluate the effect of the combination on KRAS and mTOR pathway–dependent signaling, four cell lines were treated with MRTX849 in the presence or absence of the selective ATP-competitive mTOR inhibitor vistusertib (1 μmol/L), for 6 or 24 hours, and several signaling molecules were evaluated by RPPA. Vistusertib demonstrated clear and robust inhibition of several components of the PI3K–mTOR signaling pathway including AKT (S473), p70 S6K (T412), S6 (pS235/236, S240/244), and 4E-BP1 (S65, T70) phosphorylation in each cell line at both time points consistent with its mechanism of action (Supplementary Fig. S14B). MRTX849 alone did not affect 4E-BP1 or S6 (S240/244) activity, and it exhibited a variable and cell line–dependent effect on p70 S6K and S6 (pS235/236) phosphorylation in these cell lines. Vistusertib also demonstrated marked induction of ERK phosphorylation, often several-fold over vehicle control, at both time points in all four cell lines, consistent with prior reports (30). The combination of vistusertib and MRTX849 demonstrated a comparable level of inhibition of ERK phosphorylation compared with single-agent MRTX849, indicating that the activation of ERK signaling by vistusertib was impeded by the combination of the two agents. In addition, MRTX849 combined with vistusertib further inhibited p70 S6K and AKT S473 phosphorylation compared with either single agent. Near-complete inhibition of S6 (S235/236, S240/244) phosphorylation at limit of detection was observed for the combination in each cell line at evaluated time points.

Consequently, a cohort of tumor models was identified, and the combination of MRTX849 with the selective mTOR inhibitor vistusertib demonstrated marked tumor regression and significantly improved antitumor activity compared with either single agent in all six models evaluated (Fig. 7A; Supplementary Fig. S14C). MRTX849 in combination with a second, differentiated mTOR inhibitor, everolimus, which inhibits TORC1 but not TORC2, in the H2030 xenograft model also demonstrated a striking combination effect (Supplementary Fig. S14D). In the *KRAS*^{G12C}, *STK11*-mutant H2030 model, MRTX849 demonstrated marked inhibition of ERK phosphorylation through 24 hours, but exhibited only partial inhibition of pS6$^{235/36}$ at 6 hours after dose, on days 1 and 7 (Fig. 7B and C). Vistusertib demonstrated marked inhibition of pS6$^{235/36}$ at 6 hours after treatment with evidence of recovery by 24 hours. The combination of vistusertib and MRTX849 did not have a further effect on ERK phosphorylation but demonstrated a significant reduction in pS6$^{235/36}$ on day 1 at 24 hours compared with vistusertib alone and a trend toward reduced pS6$^{235/36}$ on both day 1 and day 7 at 6 hours compared with either single agent (Fig. 7B; Supplementary Fig. S14E). Together, these data indicate that MRTX849 and mTOR inhibitor combination demonstrates complementary inhibition of the ERK and mTOR–S6 signaling pathways, resulting in broad antitumor activity in *KRAS*^{G12C}-mutant tumor models.

Signaling through KRAS is known to mediate cell proliferation, at least in part, through the regulation of the cyclin D family and triggering RB/E2F-dependent entry of cells into cell cycle. Loss-of-function mutations and homozygous deletions in the cell-cycle tumor suppressor *CDKN2A* (*p16*) are coincident in a subset of *KRAS*-mutant non–small cell lung cancer (NSCLC) and hyperactivate CDK4/6-dependent RB phosphorylation and cell-cycle transition. In the *CDKN2A*-null H2122 and SW1573 cell lines *in vitro*, MRTX849 demonstrated concentration-dependent partial inhibition of RB phosphorylation (pRB pS807/811) and concurrent increase in p27 in H2122 cells, but not SW1573 cells, at 24 hours (Fig. 7D; Supplementary Fig. S15A). MRTX849 in combination with the CDK4/6 inhibitor palbociclib (1 μmol/L) demonstrated near-complete inhibition of pRB in both H2122 and SW1573 cells and further induced p27 in H2122 cells. Interestingly, pS6 (S235/236) was also much more effectively suppressed by the combination in both H2122 and SW1573 cells, which is consistent with a recent report (31). RNA expression of target genes and RPPA analysis of target protein signaling events were also used as a readout of cell-cycle inhibition in the H2122 tumor model *in vivo*, and the combination of MRTX849 and palbociclib significantly inhibited E2F1 and selected E2F family target genes, induced p27 protein expression to a greater degree compared with either single agent, and further reduced the number of Ki-67–positive cells after 7 days of administration (Fig. 7E; Supplementary Fig. S15B and S15C). In addition, the combination demonstrated

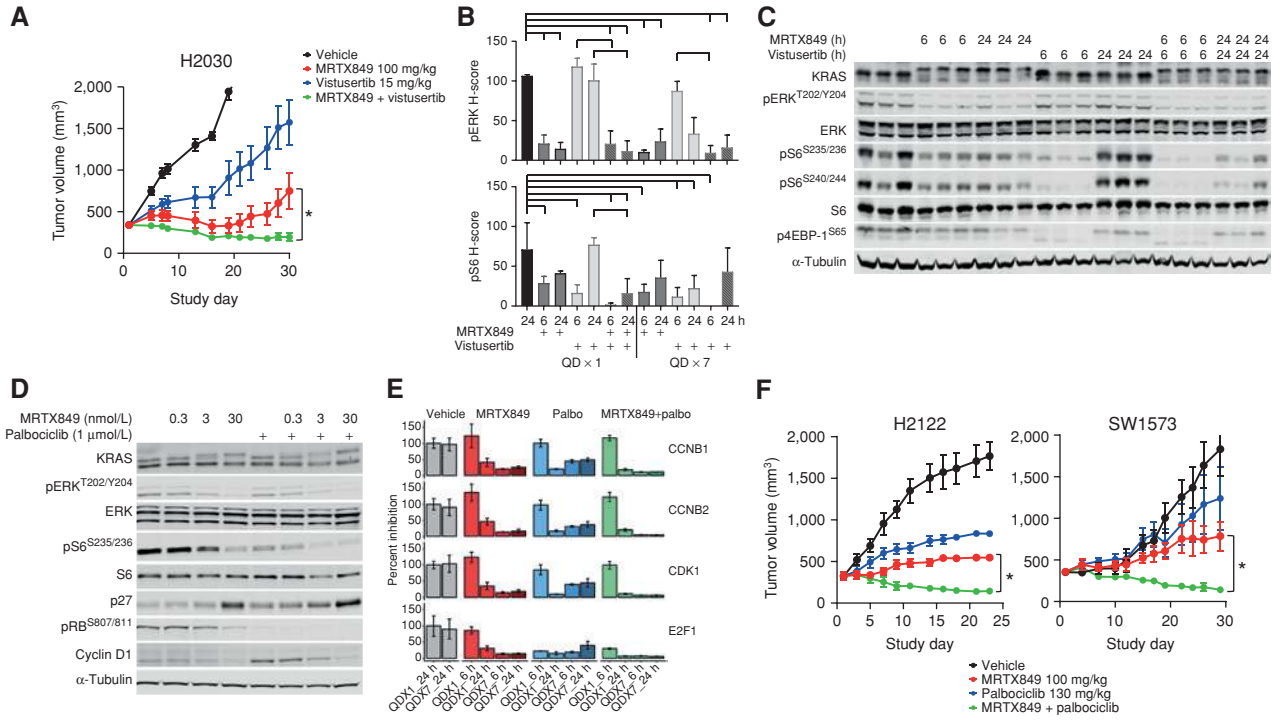

Figure 7. CDK4/6 and mTOR combinations suppress independently hyperactivated downstream pathways and exhibit increased antitumor responses. **A,** MRTX849 at 100 mg/kg, vistusertib at 15 mg/kg, or the combination was administered daily via oral gavage to mice bearing the H2122 or H2030 cell line xenografts ($n = 5$/group). Combination treatment led to a statistically significant decrease in tumor growth compared with either single-agent treatment. *, $P_{adj} < 0.05$. **B,** MRTX849 at 100 mg/kg, vistusertib at 15 mg/kg, or the combination was administered once or daily for 7 days via oral gavage to mice bearing H2030 cell line xenografts ($n = 3$/group). Tumors were harvested at 6 and 24 hours following the final dose. Tumor sections were stained with pERK and pS6 via IHC methods. Quantitation of images shown by H-score in tumor tissue. Reduction of pERK or pS6 staining intensity was determined to be statistically significant relative to vehicle or either single agent using one-way ANOVA. Brackets indicate $P < 0.05$ compared with left-most sample. **C,** Protein Western blot analysis of KRAS pathway targets in H2030 xenografts treated with MRTX849 (100 mg/kg), vistusertib (15 mg/kg), or the combination, 6 or 24 hours after a single dose. **D,** Protein Western blot analysis of KRAS pathway and cell-cycle targets in H2122 cells treated for 24 hours with MRTX849, palbociclib, or the combination. **E,** Normalized RNA-seq gene-expression data on E2F targets in H2122 xenografts treated with MRTX849, palbociclib, or the combination, 6 and 24 hours after a single daily dose or seven daily doses. **F,** MRTX849 at 100 mg/kg, palbociclib at 130 mg/kg, or the combination was administered daily via oral gavage to mice bearing the H2122 or SW1573 cell line xenografts ($n = 5$). Combination treatment led to a statistically significant decrease in tumor growth compared with either single-agent treatment. *, $P_{adj} < 0.05$.

a significant decrease in pRB (S780) compared with either single agent after 7 days of administration in SW1573 tumors *in vivo* (Supplementary Fig. S15D). This combination also induced tumor regression in five tumor xenograft models that was significant compared with either single-agent control (Fig. 7F; Supplementary Fig. S15E). Although not significant, a trend was noted in which models with *CDKN2A* homozygous deletion exhibited an increased antitumor response to the combination of MRTX849 and CDK4/6 inhibition compared with models lacking evidence of genetic dysregulation of key cell-cycle genes (Supplementary Fig. S15F and S15G).

DISCUSSION

The identification of MRTX849 as a highly selective KRAS^{G12C} inhibitor capable of near-complete inhibition of KRAS *in vivo* provides a renewed opportunity to better understand the role of this mutation as an oncogenic driver in various cancers and to guide rational clinical trial design. The lack of a significant correlation between sensitivity to MRTX849 antitumor activity in *in vitro* versus *in vivo* model systems made it necessary to further study KRAS oncogene dependence in tumor models *in vivo*, a more clinically relevant setting. The demonstration that MRTX849 exhibited significant antitumor efficacy in all evaluated *KRAS*^{G12C}-mutated cancer models and demonstrated marked regression in the majority (65%) confirms that this mutation is a broadly operative oncogenic driver and that MRTX849 represents a compelling therapeutic opportunity. This evidence of activity extended to patients, as demonstrated by RECIST partial responses in 2 patients enrolled in a phase I clinical trial of MRTX849. Collectively however, these data also illustrate that the degree of dependence of cancer cells on the presence of a *KRAS*^{G12C} mutation for growth and survival can vary across tumors and that co-occurring genetic alterations observed in *KRAS*-mutated cancers may influence response to direct targeted therapy. The further observation that *KRAS* mutations occur across different cancers and that no single co-occurring genetic alteration predicted response to treatment illustrates the genetic heterogeneity of KRAS-driven cancers. Findings in the present studies are consistent with other functional genomics or therapeutic strategies to block KRAS function

across panels of cell lines or models which demonstrated a highly significant response of *KRAS*-mutant cells to target knockdown, a heterogeneous magnitude of response, and no clear co-occurring aberrations that predict resistance to target blockade (5, 32, 33). Interestingly, despite the implication that certain mutations that co-occur with KRAS including *TP53, STK11,* and *KEAP1* may limit therapeutic response in *KRAS*^{G12C}-positive lung cancers, none of these mutations correlated with response or resistance in the cell-line panel. In addition, the partial response we reported in the patient with lung adenocarcinoma was observed in a patient harboring deleterious comutations in both *STK11* and *KEAP1*. Together, these data further illustrate the heterogeneity and complexity of *KRAS*-mutated cancers and suggest that no binary co-occurring genetic event may be predictive of therapeutic response.

Temporal and dose–response analysis indicated maximal modification of KRAS^{G12C} and durable inhibition of KRAS-dependent signaling was important in maximizing therapeutic response. The recovery of ERK signaling and the inability to inhibit mTOR–S6 signaling despite continued treatment were each associated with transient or submaximal response to MRTX849. ERK1/2 is implicated in direct phosphorylation and negative feedback regulation of EGFR (T669), FGFR1 (S777), and SOS1, and each of these targets may facilitate KRAS^{G12C}-independent resetting of ERK signaling flux (34–36). The rapid and remarkable suppression of ERK pathway–regulated transcripts such as DUSP and SPRY/SPRED family members by MRTX849 in all models evaluated is consistent with that observed for RAF inhibitors and is implicated in reactivation of ERK and RTK signaling (18, 19). The dual-specificity phosphatases DUSP4 and 6 were strongly suppressed by MRTX849 and are implicated in dephosphorylating and inactivating ERK1/2 (14, 18, 37), whereas SPRY family members are implicated in the negative regulation of RTKs and adaptor proteins (e.g., GRB2), and may participate in modifying RAS family nucleotide exchange and effector binding (e.g., RAF1; ref. 38). Although suppression of DUSP and SPRY/SPRED was broadly observed in all models, the magnitude of signaling reactivation and response to MRTX849 varied across models. This suggests some tumor models harbor additional factors that bypass KRAS dependence or affect RAS pathway signaling flux, such as expression or activation of selected RTKs (e.g., *ERBB2* amplification in the KYSE-410 model) or *STK11* loss-of-function mutations, and may be primed for feedback reactivation of RAS-dependent signaling and/or limit the degree of signaling inhibition by MRTX849. This phenomenon was observed for *BRAF*^{V600E}-mutant colon cancer (but not melanoma) which exhibits high baseline EGFR expression, is primed for rapid feedback activation of this RTK, and is resistant to single-agent inhibition but highly responsive to cotargeting BRAF (and/or MEK) and EGFR (20). In addition, blockade of BRAF or MEK1/2 resulted in feedback-mediated activation of the PI3K–mTOR signaling pathway in concert with the coactivation of upstream RTKs (e.g., EGFR), resulting in bypass of ERK pathway dependence and therapeutic resistance (17, 20, 39). The observations that baseline expression of HER family RTKs trended with MRTX849 antitumor activity and that CRISPR-based drug-anchored screens implicated EGFR, SHP2, and mTOR–S6 pathways as cotargetable vulnerabilities both support the hypothesis that these targets act as conditional response modifiers.

Activation of RTK signaling in the context of *KRAS*^{G12C}-mutant cancer was predicted to limit MRTX849 therapeutic response both by enhancing extrinsic regulation of GTPase activity and initiating KRAS-independent ERK and mTOR–S6 pathway activation. Therefore, HER family and SHP2 inhibition were employed as strategies to either block the critical RTK family in KRAS-mutant cells or block collective RTK signaling downstream, respectively. As MRTX849 binds only GDP-KRAS^{G12C}, both HER family and SHP2 inhibition each enhanced KRAS^{G12C} modification by MRTX849 and significantly improved antitumor activity. This observation is consistent with the putative role of activated RTKs in the engagement of SHP2 to mediate SOS1-dependent RAS GTP loading and to diminish RAS GAP activity, each of which converge on enhanced RAS activation state (40). The afatinib combination demonstrated a clear and marked inhibition of both the ERK–RSK and AKT–mTOR–S6 signaling pathways, whereas the SHP2 inhibitor combination demonstrated a clear impact on ERK–RSK signaling and a relatively less prominent impact on mTOR–S6 signaling. Although afatinib may more effectively address mTOR–S6 bypass signaling, SHP2 inhibition should be an effective combinatorial strategy to combat other RTKs outside of the HER family, such as FGFRs or MET, that could affect KRAS dependence. To further address bypass signaling mediated by RTK activation or *STK11* mutations, each of which activate the mTOR–S6 signaling pathway independently of KRAS, mTOR inhibition in combination with MRTX849 was also evaluated. MRTX849 in combination with vistusertib, in fact, demonstrated significantly improved antitumor activity *in vivo* compared with either single agent in all six tumor models evaluated, regardless of *STK11* mutational status. Consistent with the mechanism of action of vistusertib, comprehensive inhibition of AKT–mTOR–S6 signaling was observed for vistusertib alone and near-complete inhibition of pS6$^{S235-36}$ and pS6$^{240-44}$ was observed in combination. In addition, the marked feedback reactivation of ERK by vistusertib was relieved by the combination. The induction of ERK activity has been observed in tumor cells following mTORC1 inhibition by rapalogs or ATP-competitive inhibitors and has been implicated in limiting antitumor activity of this class of agents (30, 41, 42), supporting the suppression of ERK signaling by MRTX849 as a key mechanism of response to the combination. Notably, all three combination strategies converge on more comprehensive inhibition of KRAS-dependent signaling, converging on ERK and S6 activity. In addition, although the inhibition of the AKT–mTOR–S6 pathway did not correlate with model response to MRTX849 (potentially due to tumor heterogeneity), the observations that both MTOR and RPS6 drop out in drug-anchored CRISPR screens and that effective combination strategies more comprehensively block this pathway illustrate its likely importance in maximizing therapeutic response in *KRAS*-mutated cancers.

Cell-cycle dysregulation due to genetic alterations in cell-cycle regulators identified additional factors that could

modify the therapeutic response to MRTX849. In addition, *CDKN2A, RB1, CDK4,* and *CDK6* were all identified as gene targets that affected cell fitness in CRISPR screens. Genetic alterations including homozygous deletion of *CDKN2A* or amplification of *CDK4* or *CCND1* comprise up to 20% of *KRAS*-mutated NSCLC (43). Combination studies with MRTX849 and palbociclib *in vivo* demonstrated more comprehensive inhibition of RB and E2F family target genes and increased antitumor activity compared with either single agent in NSCLC models. In addition, these studies indicated that the combination resulted in more effective inhibition of S6 (S235/236) phosphorylation, establishing a previously unappreciated connection between cell-cycle blockade and protein translation pathways. Notably, this combination was especially effective in *CDKN2A*-deleted models, suggesting that this combination strategy may be primarily beneficial in a molecularly defined subset of patients characterized by decoupling of cell-cycle regulation from KRAS.

Collectively, models exhibiting a cytoreductive response to single-agent MRTX849 demonstrated a more comprehensive and durable inhibition of KRAS-dependent signaling and induction of an apoptotic response. These data suggest that maintaining durable inhibition of KRAS-dependent signaling below a defined threshold is required to elicit tumor regression. The elucidation of mechanisms that limit the therapeutic response to single-agent KRAS inhibition has provided insight toward strategies to enhance therapeutic activity in *KRAS*-mutant tumors. Of the 35% of models (9/26) that did not exhibit durable regression with single-agent MRTX849 treatment, five models (KYSE410, SW1573, H2122, H2030, and LU6405) were selected for rational combination studies, and at least one combination demonstrated significant improvement in antitumor efficacy and elicited a >50% tumor regression in all five models evaluated. These results suggest that essentially all $KRAS^{G12C}$-mutated cancers can derive clinical benefit from direct KRAS inhibitor–directed therapy either alone or in combination. Furthermore, rational pathway-centric combination regimens directed at hallmark signaling nodes may be directed to genetically defined patient subsets. For example, *KRAS*-mutated NSCLC exhibits mutually exclusive, co-occurring genetic alterations in *STK11* and *CDKN2A* (43). The present data suggest that $KRAS^{G12C}$/*STK11*-mutated NSCLC could be readily addressed by combining a $KRAS^{G12C}$ inhibitor with an RTK or mTOR inhibitor, whereas $KRAS^{G12C}$/*CDKN2A*-mutated NSCLC could be more effectively addressed by combination with a CDK4/6 inhibitor. Collectively, the present studies support the broad utility of covalent $KRAS^{G12C}$ inhibitors in treating $KRAS^{G12C}$-mutated cancers and provide defining strategies to identify patients likely to benefit from single-agent therapy or rationally directed combinations.

METHODS

Reagents and Cell Lines

MRTX849 was synthesized at Array Biopharma, Inc., or WuXi AppTec. MRTX849 in powder form was stored at room temperature and protected from light. MRTX849 was formulated in 100% DMSO and aliquoted for long-term storage at −20°C. RPMI-1640 medium (#11875-093), DMEM (#10566-016), penicillin and streptomycin (#15070-063), HEPES [(4-(2-hydroxyethyl)-1-piperazineethanesulfonic acid); #15630-080], Dulbecco's Phosphate-Buffered Saline (#14190-136), and sodium pyruvate (#11360-070) were obtained from Gibco/Thermo Fisher Scientific. FBS was obtained from Corning (#35-011-CV) and Nucleus Biologics (1824-001). MIA PaCa-2, NCI-H358, SW837, NCI-H2122, SW756, Calu-1, SW1573, NCI-H1373, NCI-H2030, NCI-H1792, NCI-H23, UM-UC-3, A549, H1299, and HCT 116 cell lines were obtained from the ATCC between April 2014 and August 2015. Cell lines are abbreviated without the NCI prefix for brevity. The HCC-44 cell line was obtained in August 2015 from Deutsche Sammlung von Mikroorganismen und Zellkulturen. The LU99, LU65, and IALM cell lines were obtained in September 2017 from RIKEN. The KYSE-410 cell line was obtained in August 2015 from Sigma/Millipore. Human cancer cell lines were maintained at 37°C in a humidified incubator at 5% CO_2 and were periodically checked for *Mycoplasma*. Cell lines used for *in vivo* studies were confirmed pathogen and *Mycoplasma*-free by IMPACT 1 assessment (IDEXX BioAnalytics) prior to implant. Cell lines were carried for no more than 15 cell passages in this work.

In Vivo *Studies*

All mouse studies were conducted in compliance with all applicable regulations and guidelines of the Institutional Animal Care and Use Committee from the NIH. Mice were maintained under pathogen-free conditions, and food and water was provided *ad libitum*. Six- to 8-week-old, female, athymic nude-*Foxn1*^{nu} mice (Envigo) were injected subcutaneously with tumor cells in 100 μL of PBS and Matrigel matrix in the right hind flank with 5.0e6 cells (Corning #356237; Discovery Labware) 50:50 cells:Matrigel. Mouse health was monitored daily, and caliper measurements began when tumors were palpable. Tumor volume measurements were determined utilizing the formula $0.5 \times L \times W^2$ in which L refers to length and W refers to width of each tumor. When tumors reached an average tumor volume of approximately 350 to 400 mm^3, mice were randomized into treatment groups. Mice were treated by oral gavage with either vehicle consisting of 10% research grade Captisol (CyDex Pharmaceuticals) in 50 mmol/L citrate buffer pH 5.0 or MRTX849 in vehicle at indicated doses. For efficacy studies, animals were orally administered MRTX849 or vehicle and monitored daily, tumors were measured 3 times per week, and body weights were measured 2 times per week. Study day on efficacy plots indicates the day after which MRTX849 treatment was initiated.

For studies conducted at Crown Biosciences China, 4- to 5-week-old female BALB/c nude mice were implanted with tumor fragments 2 to 3 mm in diameter into the right flank via trocar implant.

For studies conducted at Crown Biosciences San Diego, tumor cells were thawed, washed in PBS, counted, and resuspended in cold PBS at between approximately 50,000 and 100,000 cells per 100 μL. Cell suspensions were mixed with an equal volume of Cultrex extracellular matrix (ECM; Trevigen; #3432-005-01) and kept on ice. Six- to 8-week-old, female, NOD/SCID mice were shaved prior to injection, and 100 μL of the ECM–cell mixture was injected in the rear flank using a chilled 26 7/8-gauge syringe.

Mice were randomized, and dosing was initiated when the mean tumor volume was between approximately 250 and 300 mm^3. Five mice were dosed with either vehicle alone (10% Captisol in 10 mmol/L citrate buffer, pH 5.0; Teknova; #Q2443) or 100 mg/kg MRTX849 daily by oral gavage for 21 days ($n = 5$ per group).

Statistical analysis of differences in mean tumor volume between vehicle- and MRTX849-treated cohorts was run using a two-tailed Student t test with equal variance in Excel (Microsoft). P value < 0.05 was considered statistically significant.

Clinical Trials

MRTX849 clinical trials (NCT03785249) were conducted in accordance with recognized U.S. ethical guidelines (i.e., U.S. Common Rule) and per local institutional review board guidelines. All patients included in the clinical trial were subjected to informed written consent and consented prior to study enrollment. MRTX849 was administered in 21-day cycles to patients included in the present studies per protocol.

Disclosure of Potential Conflicts of Interest

J.G. Christensen is CSO of Mirati Therapeutics and has ownership interest (including patents) in the same. J. Hallin, L.D. Engstrom, and D.M. Briere are principal scientists at Mirati Therapeutics and have ownership interest (including patents) in the same. L. Hargis is an associate scientist at Mirati Therapeutics. A. Calinisan and V. Bowcut are associate scientists at Mirati Therapeutics and have ownership interest (including patents) in the same. R. Aranda is a scientist at Mirati Therapeutics and has ownership interest (including patents) in the same. N. Sudhakar is a scientist at Mirati Therapeutics. J.A. Ballard is a research investigator at Array Biopharma and has ownership interest (including patents) in Mirati Therapeutics. M.R. Burkard is a senior research scientist at Array Biopharma Inc. and Pfizer Inc. and has ownership interest (including patents) in Pfizer Inc. J.P. Fischer is a research investigator at Array Biopharma and has ownership interest (including patents) in the same. G.P. Vigers is a research fellow at Array Biopharma and has ownership interest (including patents) in the same. S. Gatto is an employee at Monoceros Biosystems LLC. J. Fernandez-Banet is a principal scientist at Monoceros Biosystems LLC. A. Pavlicek is a CEO at Monoceros Biosystems LLC and has ownership interest (including patents) in Mirati Therapeutics. K. Velastegui is a clinical scientist at Mirati Therapeutics and has ownership interest (including patents) in the same. R.C. Chao is an executive medical director at Mirati Therapeutics and has ownership interest (including patents) in the same. J. Barton is a chief medical officer at Mirati Therapeutics and has ownership interest (including patents) in the same. M. Pierobon has ownership interest (including patents) in Theranostics Health. E.F. Patricoin III is a chief science officer at, has ownership interest (including patents) in, and has an unpaid consultant/advisory board relationship with Perthera, Inc. M.A. Marx is a VP, Drug Discovery, at Mirati Therapeutics and has ownership interest (including patents) in the same. M.L. Johnson has a consulting/advisory role at Otsuka, Astellas Pharma, Mirati, Araxes Pharma, Mersana, Beigene, Incyte, Pfizer, Guardant Health, Bristol-Myers Squibb, Ribon, Genentech/Roche, Celgene, Boehringer Ingelheim, AstraZeneca, Calithera Biosciences, Merck, Loxo, and Sanofi; reports receiving research funding from OncoMed, BerGenBio, Lilly, EMD Serono, Kadmon, Janssen, Mirati, Genmab, Pfizer, AstraZeneca, SemCentRx, Novartis, Checkpoint Therapeutics, Array BioPharma, Regeneron, Merck, Hengrui Pharmaceutical, Lycera, BeiGene, Tarveda Therapeutics, Loxo, AbbVie, Boehringer Ingelheim, Guardant Health, Foundation Medicine, Sanofi, Mersana, Cytomx Therapeutics, Dynavax, Birdie, Corvus, Incyte, Genocea Biosciences, Gritstone Oncology, Amgen, Genentech/Roche, AdaptImmune, Syndax, Neovia Oncology, G1 Therapeutics, Bristol-Myers Squibb, Clovis, and Acera; and reports receiving travel/accommodations/expenses from AbbVie, Astellas Pharma, AstraZeneca, Boehringer Ingelheim, Clovis Oncology, Daiichi Sankyo, EMD Serono, Bristol-Myers Squibb, Exelixis, Genentech, Incyte, Merck, Pfizer, Sysmex, and Vapotherm. S.-H.I. Ou is a consultant at AstraZeneca, is a consultant/advisory board member for Roche/Genentech, is a member of the scientific board at Turning Point Therapeutics, reports receiving honoraria from the speakers' bureaus of Pfizer, AstraZeneca, Takeda, and Roche/Genentech, and has ownership interest (including patents) in Turning Point Therapeutics. P. Lito reports receiving commercial research support from Mirati Therapeutics. P.A. Jänne is a consultant at AstraZeneca, Boehringer Ingelheim, SFJ Pharmaceuticals, Daiichi Sankyo, Takeda Oncology, Pfizer, Roche/Genentech, Chugai, ACEA Biosciences, Ignyta, Eli Lilly, and Araxes; is a SAB at Voronoi and Biocartis; is a consultant/SAB at Mirati Therapeutics and Loxo Oncology; reports receiving commercial research grants from AstraZeneca, Boehringer Ingelheim, Astellas Pharmaceuticals, PUMA, Daiichi Sankyo, Eli Lilly, and Takeda Oncology; has ownership interest (including patents) in Gatekeeper Pharmaceuticals and LOXO Oncology; and has received other remuneration from LabCorp. P. Olson is a senior director of research at Mirati Therapeutics and has ownership interest (including patents) in the same. No potential conflicts of interest were disclosed by the other authors.

Authors' Contributions

Conception and design: J. Hallin, L.D. Engstrom, L. Hargis, R. Aranda, J.B. Fell, J.P. Fischer, M.A. Marx, P. Olson, J.G. Christensen

Development of methodology: J. Hallin, L.D. Engstrom, L. Hargis, A. Calinisan, R. Aranda, D.M. Briere, N. Sudhakar, J.A. Ballard, M.R. Burkard, G.P. Vigers, E.F. Petricoin III, M.A. Marx, P. Olson, J.G. Christensen

Acquisition of data (provided animals, acquired and managed patients, provided facilities, etc.): J. Hallin, L.D. Engstrom, L. Hargis, A. Calinisan, R. Aranda, D.M. Briere, N. Sudhakar, B.R. Baer, J.A. Ballard, Y. Xue, M. Pierobon, E. Baldelli, E.F. Petricoin III, D.P. Cassidy, I.I. Rybkin, S.-H.I. Ou, P. Lito, K.P. Papadopoulos, P.A. Jänne

Analysis and interpretation of data (e.g., statistical analysis, biostatistics, computational analysis): J. Hallin, L.D. Engstrom, L. Hargis, A. Calinisan, R. Aranda, D.M. Briere, N. Sudhakar, V. Bowcut, B.R. Baer, J.A. Ballard, S. Gatto, J. Fernandez-Banet, A. Pavlicek, E.F. Petricoin III, I.I. Rybkin, S.-H.I. Ou, P. Lito, K.P. Papadopoulos, P.A. Jänne, P. Olson, J.G. Christensen

Writing, review, and/or revision of the manuscript: J. Hallin, L.D. Engstrom, L. Hargis, D.M. Briere, N. Sudhakar, B.R. Baer, M.R. Burkard, J.B. Fell, S. Gatto, J. Fernandez-Banet, A. Pavlicek, K. Velastagui, R.C. Chao, J. Barton, E.F. Petricoin III, M.A. Marx, I.I. Rybkin, M.L. Johnson, S.-H.I. Ou, P. Lito, K.P. Papadopoulos, P.A. Jänne, P. Olson, J.G. Christensen

Administrative, technical, or material support (i.e., reporting or organizing data, constructing databases): J. Hallin, L.D. Engstrom, L. Hargis, R. Aranda, N. Sudhakar, K. Velastagui, E.F. Petricoin III, D.P. Cassidy, P. Olson

Study supervision: J. Hallin, L.D. Engstrom, K.P. Papadopoulos, P. Olson, J.G. Christensen

Other (Med chemistry for 849): J.P. Fischer

Acknowledgments

The authors thank Channing J. Der and Adrienne D. Cox for critical review of the manuscript. The authors thank Molecular Diagnostic Services and Crown Biosciences for animal study support and Flagship Biosciences for IHC and image analysis. Support for collaborative research to evaluate the impact of KRAS comutations on KRAS inhibitor activity with the Lito laboratory was provided, in part, by NIH/NCI (1R01CA23074501; 1R01CA23026701A1), The Pew Charitable Trusts, and the Damon Runyon Cancer Research Foundation. J. Xue is supported by a National Research Service Award from the NIH/NCI (1F30CA232549-01).

The costs of publication of this article were defrayed in part by the payment of page charges. This article must therefore be hereby marked *advertisement* in accordance with 18 U.S.C. Section 1734 solely to indicate this fact.

Received October 6, 2019; revised October 18, 2019; accepted October 18, 2019; published first October 28, 2019.

REFERENCES

1. John J, Sohmen R, Feuerstein J, Linke R, Wittinghofer A, Goody RS. Kinetics of interaction of nucleotides with nucleotide-free H-ras p21. Biochemistry 1990;29:6058–65.
2. Matikas A, Mistriotis D, Georgoulias V, Kotsakis A. Targeting KRAS mutated non-small cell lung cancer: a history of failures and a future of hope for a diverse entity. Crit Rev Oncol Hematol 2017;110: 1–12.
3. Sanchez-Vega F, Mina M, Armenia J, Chatila WK, Luna A, La KC, et al. Oncogenic signaling pathways in the cancer genome atlas. Cell 2018;173:321–37.
4. Simanshu DK, Nissley DV. McCormick F. RAS proteins and their regulators in human disease. Cell 2017;170:17–33.
5. Janes MR, Zhang J, Li LS, Hansen R, Peters U, Guo X, et al. Targeting KRAS mutant cancers with a covalent G12C-specific inhibitor. Cell 2018;172:578–89.
6. Ostrem JM, Peters U, Sos ML, Wells JA, Shokat KM. K-Ras(G12C) inhibitors allosterically control GTP affinity and effector interactions. Nature 2013;503:548–51.
7. Patricelli MP, Janes MR, Li LS, Hansen R, Peters U, Kessler LV, et al. Selective inhibition of oncogenic KRAS output with small molecules targeting the inactive state. Cancer Discov 2016;6:316–29.
8. Ambrogio C, Kohler J, Zhou ZW, Wang H, Paranal R, Li J, et al. KRAS dimerization impacts MEK inhibitor sensitivity and oncogenic activity of mutant KRAS. Cell 2018;172:857–68.
9. Burgess MR, Hwang E, Mroue R, Bielski CM, Wandler AM, Huang BJ, et al. KRAS allelic imbalance enhances fitness and modulates MAP kinase dependence in cancer. Cell 2017;168:817–29.
10. Cancer Genome Atlas Network. Comprehensive molecular characterization of human colon and rectal cancer. Nature 2012;487: 330–7.
11. Schabath MB, Welsh EA, Fulp WJ, Chen L, Teer JK, Thompson ZJ, et al. Differential association of STK11 and TP53 with KRAS mutation-associated gene expression, proliferation and immune surveillance in lung adenocarcinoma. Oncogene 2016;35:3209–16.
12. Skoulidis F, Goldberg ME, Greenawalt DM, Hellmann MD, Awad MM, Gainor JF, et al. STK11/LKB1 mutations and PD-1 inhibitor resistance in KRAS-mutant lung adenocarcinoma. Cancer Discov 2018;8:822–35.
13. Brant R, Sharpe A, Liptrot T, Dry JR, Harrington EA, Barrett JC, et al. Clinically viable gene expression assays with potential for predicting benefit from MEK inhibitors. Clin Cancer Res 2017;23:1471–80.
14. Caunt CJ, Keyse SM. Dual-specificity MAP kinase phosphatases (MKPs): shaping the outcome of MAP kinase signalling. FEBS J 2013;280:489–504.
15. Merchant M, Moffat J, Schaefer G, Chan J, Wang X, Orr C, et al. Combined MEK and ERK inhibition overcomes therapy-mediated pathway reactivation in RAS mutant tumors. PLoS One 2017;12: e0185862.
16. Sturm OE, Orton R, Grindlay J, Birtwistle M, Vyshemirsky V, Gilbert D, et al. The mammalian MAPK/ERK pathway exhibits properties of a negative feedback amplifier. Sci Signal 2010;3:ra90.
17. Turke AB, Song Y, Costa C, Cook R, Arteaga CL, Asara JM, et al. MEK inhibition leads to PI3K/AKT activation by relieving a negative feedback on ERBB receptors. Cancer Res 2012;72:3228–37.
18. Lito P, Pratilas CA, Joseph EW, Tadi M, Halilovic E, Zubrowski M, et al. Relief of profound feedback inhibition of mitogenic signaling by RAF inhibitors attenuates their activity in BRAFV600E melanomas. Cancer Cell 2012;22:668–82.
19. Lito P, Rosen N, Solit DB. Tumor adaptation and resistance to RAF inhibitors. Nat Med 2013;19:1401–9.
20. Prahallad A, Sun C, Huang S, Di Nicolantonio F, Salazar R, Zecchin D, et al. Unresponsiveness of colon cancer to BRAF(V600E) inhibition through feedback activation of EGFR. Nature 2012;483:100–3.
21. Chandarlapaty S, Sawai A, Scaltriti M, Rodrik-Outmezguine V, Grbovic-Huezo O, Serra V, et al. AKT inhibition relieves feedback suppression of receptor tyrosine kinase expression and activity. Cancer Cell 2011;19:58–71.
22. Misale S, Fatherree JP, Cortez E, Li C, Bilton SJ, Timonina D, et al. KRAS G12C NSCLC models are sensitive to direct targeting of KRAS in combination with PI3K inhibition. Clin Cancer Res 2019;25: 769–807.
23. Hunter JC, Manandhar A, Carrasco MA, Gurbani D, Gondi S, Westover KD. Biochemical and structural analysis of common cancer-associated KRAS mutations. Mol Cancer Res 2015;13:1325–35.
24. Lito P, Solomon M, Li LS, Hansen R, Rosen N. Allele-specific inhibitors inactivate mutant KRAS G12C by a trapping mechanism. Science 2016;351:604–8.
25. Mainardi S, Mulero-Sanchez A, Prahallad A, Germano G, Bosma A, Krimpenfort P, et al. SHP2 is required for growth of KRAS-mutant non-small-cell lung cancer in vivo. Nat Med 2018;24:961–7.
26. Nichols RJ, Haderk F, Stahlhut C, Schulze CJ, Hemmati G, Wildes D, et al. RAS nucleotide cycling underlies the SHP2 phosphatase dependence of mutant BRAF-, NF1- and RAS-driven cancers. Nat Cell Biol 2018;20:1064–73.
27. Ruess DA, Heynen GJ, Ciecielski KJ, Ai J, Berninger A, Kabacaoglu D, et al. Mutant KRAS-driven cancers depend on PTPN11/SHP2 phosphatase. Nat Med 2018;24:954–60.
28. Baldelli E, Bellezza G, Haura EB, Crino L, Cress WD, Deng J, et al. Functional signaling pathway analysis of lung adenocarcinomas identifies novel therapeutic targets for KRAS mutant tumors. Oncotarget 2015;6:32368–79.
29. Roux PP, Shahbazian D, Vu H, Holz MK, Cohen MS, Taunton J, et al. RAS/ERK signaling promotes site-specific ribosomal protein S6 phosphorylation via RSK and stimulates cap-dependent translation. J Biol Chem 2007;282:14056–64.
30. Rastogi R, Jiang Z, Ahmad N, Rosati R, Liu Y, Beuret L, et al. Rapamycin induces mitogen-activated protein (MAP) kinase phosphatase-1 (MKP-1) expression through activation of protein kinase B and mitogen-activated protein kinase kinase pathways. J Biol Chem 2013;288:33966–77.
31. Lou K, Steri V, Ge AY, Hwang YC, Yogodzinski CH, Shkedi AR, et al. KRAS(G12C) inhibition produces a driver-limited state revealing collateral dependencies. Sci Signal 2019;12.
32. McDonald ER III, de Weck A, Schlabach MR, Billy E, Mavrakis KJ, Hoffman GR, et al. Project DRIVE: a compendium of cancer dependencies and synthetic lethal relationships uncovered by large-scale, deep RNAi screening. Cell 2017;170:577–92.
33. Tsherniak A, Vazquez F, Montgomery PG, Weir BA, Kryukov G, Cowley GS, et al. Defining a cancer dependency map. Cell 2017;170:564–76.
34. Li X, Huang Y, Jiang J, Frank SJ. ERK-dependent threonine phosphorylation of EGF receptor modulates receptor downregulation and signaling. Cell Signal 2008;20:2145–55.
35. Porfiri E, McCormick F. Regulation of epidermal growth factor receptor signaling by phosphorylation of the ras exchange factor hSOS1. J Biol Chem 1996;271:5871–7.
36. Zakrzewska M, Haugsten EM, Nadratowska-Wesolowska B, Oppelt A, Hausott B, Jin Y, et al. ERK-mediated phosphorylation of fibroblast growth factor receptor 1 on Ser777 inhibits signaling. Sci Signal 2013;6:ra11.
37. Huang CY, Tan TH. DUSPs, to MAP kinases and beyond. Cell Biosci 2012;2:24.
38. Hanafusa H, Torii S, Yasunaga T, Nishida E. Sprouty1 and Sprouty2 provide a control mechanism for the Ras/MAPK signalling pathway. Nat Cell Biol 2002;4:850–8.
39. Villanueva J, Vultur A, Lee JT, Somasundaram R, Fukunaga-Kalabis M, Cipolla AK, et al. Acquired resistance to BRAF inhibitors mediated by a RAF kinase switch in melanoma can be overcome by cotargeting MEK and IGF-1R/PI3K. Cancer Cell 2010;18:683–95.

40. Zhang J, Zhang F, Niu R. Functions of Shp2 in cancer. J Cell Mol Med 2015;19:2075–83.
41. Svejda B, Kidd M, Kazberouk A, Lawrence B, Pfragner R, Modlin IM. Limitations in small intestinal neuroendocrine tumor therapy by mTor kinase inhibition reflect growth factor-mediated PI3K feedback loop activation via ERK1/2 and AKT. Cancer 2011;117:4141–54.
42. Zeng Y, Tian X, Wang Q, He W, Fan J, Gou X. Attenuation of everolimus-induced cytotoxicity by a protective autophagic pathway involving ERK activation in renal cell carcinoma cells. Drug Des Devel Ther 2018;12:911–20.
43. Zehir A, Benayed R, Shah RH, Syed A, Middha S, Kim HR, et al. Mutational landscape of metastatic cancer revealed from prospective clinical sequencing of 10,000 patients. Nat Med 2017;23:703–13.